RSC Advances

PAPER

View Article Online
View Journal | View Issue

Cite this: *RSC Adv.*, 2024, **14**, 13062

Bioactive O^N^O^ Schiff base appended homoleptic titanium(IV) complexes: DFT, BSA/CT-DNA interactions, molecular docking and antitumor activity against HeLa and A549 cell lines†

Sathish Thanigachalam and Madhvesh Pathak *

Five new homoleptic derivatives of titanium(IV) have been developed and characterized by physicochemical techniques. Metal complexes, TiH_2L^1 [$(C_{38}H_{26}N_6O_4)Ti$], TiH_2L^2 [$(C_{38}H_{24}F_2N_6O_4)Ti$], TiH_2L^3 [$(C_{38}H_{24}Cl_2N_6O_4)Ti$], TiH_2L^4 [$(C_{38}H_{24}Br_2N_6O_4)Ti$] and TiH_2L^5 [$(C_{38}H_{24}N_8O_8)Ti$], were obtained by treating $Ti(OPr^i)_4$ with appropriate ONO ligands (H_2L^1–H_2L^5) in anhydrous THF as solvent. The electronic structures and properties of titanium(IV) complexes (TiH_2L^1–TiH_2L^5) and ligands (H_2L^1–H_2L^5) were examined by DFT studies. The stability of all synthesized derivatives was assessed by a UV-visible technique using 10% DMSO, GSH medium and *n*-octanol/water systems. The binding interactions of BSA and CT-DNA with respective titanium(IV) complexes were successfully evaluated by employing UV-visible absorption, fluorescence, circular dichroism (CD) techniques and docking studies. The *in vitro* cytotoxicity of TiH_2L^2, TiH_2L^3 and TiH_2L^4 complexes was assessed against HeLa (human epithelioid cervical cancer cells) and A549 (lung carcinoma) cell lines. The IC_{50} values of TiH_2L^2, TiH_2L^3 and TiH_2L^4 were observed to be 28.8, 14.7 and 31.2 μg mL^{-1} for the HeLa cell line and 38.2, 32.9 and 67.78 μg mL^{-1} for A549 cells, respectively. Complex TiH_2L^3 exhibited remarkably induced cell cycle arrest in the G_1 phase and 77.99% ROS production selectivity in the HeLa cell line.

Received 15th December 2023
Accepted 6th April 2024

DOI: 10.1039/d3ra08574k

rsc.li/rsc-advances

Department of Chemistry, School of Advanced Sciences, Vellore Institute of Technology, Vellore 632014, Tamilnadu, India. E-mail: madhveshpathak@vit.ac.in

† Electronic supplementary information (ESI) available. See DOI: https://doi.org/10.1039/d3ra08574k

Sathish Thanigachalam

Sathish T completed his BSc (2017) and MSc Chemistry (2019) at the Presidency College, Chennai, affiliated to University of Madras, Chennai, Tamil Nadu, India. Presently, he is pursuing a PhD on 'Metallo-organic complexes and their versatile applications' under the kind guidance of Dr Madhvesh Pathak, Department of Chemistry, School of Advanced Sciences, Vellore Institute of Technology (VIT), Vellore, Tamil Nadu, India.

Madhvesh Pathak

Madhvesh Pathak was graduated from Chaudhari Charan Singh University, Meerut, Uttar Pradesh, India in 1996. He pursued his MSc at the Department of Chemistry, University of Roorkee, Roorkee (Presently IIT Roorkee), Uttrakhand, India in 1998. He completed his PhD in 2004 under the kind guidance of Prof. Rakesh Bohra and Prof. Ram C. Mehrotra, Department of Chemistry, University of Rajasthan Jaipur, Rajasthan, India. He served as a lecturer in the Department of Chemistry, Jaipur Engineering College and Research Centre (JECRC), Jaipur, India from Aug 2004 to Feb 2009. Afterwards, he joined the Department of Chemistry, School of Advanced Sciences, Vellore Institute of Technology (VIT) Vellore, India in 2009 as an Assistant Professor (Sr) and presently he is working as a Professor therein. His research interests include synthetic inorganic chemistry, metallo-organic complexes and applications of complexes in the fields of catalysis, hydrophobic materials as well as in biological evaluations.

1. Introduction

Transition metals coordinated with ligands of appropriate cationic, neutral or anionic behaviour are rendered capable of being listed as transition metal complexes.[1] Transition metal derivatives with versatile coordination spheres and oxidation states easily interact with negatively charged biomolecules.[2] The first mono-nuclear cisplatin anti-cancer drug was discovered in 1969, which exhibited immortal cytotoxicity against ovary, testis, neck and lung cancer cells, but the main drawback of cisplatin, oxaliplatin and carboplatin drugs was that they caused various side effects, *e.g.* vomiting, nausea, renal disability, alopecia (hair loss), neurotoxicity and ototoxicity (reducing hearing ability).[3] During the recent couple of decades, many researchers have come up with extensive studies with results for developing non-platinum-based drugs. Further, in pursuit of the above-mentioned purpose, transition metal titanium has attracted attention because of its low toxicity and relatively high abundance in the earth's crust that furnishes desirable metal cations in the field of interest. Because of the hydrophobic nature of alkoxy groups and lower volatility of free alcohols, titanium(IV) alkoxides are frequently preferred over tetra halides, allowing safer and swifter experimental processing to develop new derivatives.[4] Tetravalent titanium(IV) complexes have entered the clinical trial stage as the first alternative non-platinum-based anti-cancer medications, *e.g.* titanocene dichloride and budotitane proposed by Köpf Mayer in 1979 had appealing possibilities in the development of effective and secure metallodrugs for the treatment of malignancy.[5–8] Two parent chemicals, cyclopentadienyl- and diketonato-based titanium(IV) complexes, were extensively investigated against various cancer cells,[8–16] and these drugs are more active than cisplatin-resistant cell lines with lesser side effects.[17,18]

Transferrin (Tf) contributes only up to 39% of Fe(III) in human blood, and it also binds with other metal ions ideally hard Lewis acids. Tf enters cells by getting transferred through transferrin receptors (TfR), which are overexpressed in cancerous cells.[19,20] The strong Lewis acidic nature of titanium(IV) classes enables it to disrupt more than 200 different biological (Lewis basic) processes in human body cell types including cancerous ones. Due to the aqueous vulnerability of titanocene dichloride, Sadler proposed that iron transport protein transferrin (Tf) would be capable of providing a 'Trojan horse' to supply exchangeable ions of Ti(IV) to quench the thirst for iron by cancer cells.[21] After the formation of a stable Ti_2–Tf complex, it was transported intracellularly to endosomes, leading to the release of Ti^{4+} ions upon coming into contact with cellular ATP and subsequent binding to DNA/RNA nucleic acid regions.[19,22]

The anticipated mechanism for the transport of Ti(IV) ions bonded with proteins involves their release within the cells by a chelating molecule. Indeed, Tf is bound with the hard acid Ti(IV) more firmly than Fe(III).[23] Subsequently, it was proposed that since cancer cells express more Tf receptors and have a higher iron requirement than normal cells, Ti(IV)-bound Tf results in two anticancer impacts: an upsurge in cytotoxic Ti(IV) consumption and the lack of necessary iron for cancer cells.[24] Three types of programmed cell death (PCD) could occur there and among those three, the foremost form is said to be apoptosis (type 1), while autophagy (type 2) and regulated necrosis (type 3) also exist.[25] All these PCDs could be distinguished by alterations in cellular morphology as well as in biochemical and biomolecular changes. Apoptosis was the most prevalent type of planned cell death that has been projected for titianocene dichloride. Apoptotic cells undergo membrane blebbing (the creation of protrusions in the cell membrane), cell shrinkage, nuclear fragmentation, DNA chromatin condensation and the formation of apoptotic bodies.[19,25,26] Titanocene dichloride is more prevalent in regions close to nuclear chromatin, where it covalently bonds to DNA and prevents further multiplication of DNA.[27] Several titanium derivatives, such as budotitane and titanocene dichloride, were not submitted to further clinical development in spite of their promising outputs in *in vivo* and *in vitro* conditions due to their intensified reactivity, side effects, ease of hydrolysis and meagre solubility in a biological environment, resulting in a wide variety of metabolites, and this has limited the further development of anticancer drug discoveries, and the properties of the active species with their mechanisms have yet to be well established.[7,12,19,28–31] When Ti(IV) halo-salan alkoxides are introduced as drugs, they induce cell death *via* apoptosis, which demonstrates that halogen-substituents have a favourable effect on aqueous stability. As initiation, MCF7 cells were exposed to a phenola Ti(IV) complex that caused apoptosis and induced cell-cycle arrest in the G_2/M phase and targeted the endoplasmic reticulum (ER)/mitochondrial pathway.[31]

Immal and co-workers synthesized different halogen-substituted salan and salane supported titanium(IV) derivatives, which exhibited significant cytotoxicity and induced apoptotic cell death.[27,32] Salan (ONNO) and thiosalan (OSSO) type associated titanium(IV) complexes displayed efficient antiproliferative activity against HeLa and Hep G2 cells, as reported by Martin Grützke *et al.*[33] Zohar Shpilt's research group developed ONO-tridentate ligand-based mono-nuclear titanium(IV) derivatives that demonstrated effective cytotoxicity against ovarian and colon cell lines.[34] Tshuva *et al.* developed new complexes of titanium(IV) coordinated with various salan ligand systems and discussed their hydrolytic stability followed by their anti-cancer activities against various carcinoma cell lines.[35–39] Significant cytotoxic studies against K562, MDA-MB-361, Fem-x and HeLa cells were carried out with diamine bis(phenolate) titanium complexes, considering their hydrolytic behaviour, as reported by Sónia Barroso *et al.* in 2014.[40] Very recently, (in 2023) a novel derivative of titanium(IV) incorporated with diaminobis(phenolato)-bis(alkoxo) ligands was also established while investigating cytotoxicity towards colon HT-29, human ovarian A2780 and HeLa cell lines.[41] Anastasia Pedko *et al.* successfully developed [ONON] diaminobis(phenolato) ligand supported titanium(IV) complexes and evaluated their antitumor activities against colon HT-29 and human ovarian A2780 cell lines with remarkable IC_{50} values (0.6–13 μM after incubation for 72 h).[42] In 2019, budotitane-

based hexa-coordinated Ti(IV) derivatives were tested against C6 (glioma), CHO (Chinese hamster ovarian) and HeLa cell lines (5.6–6.2 μM).[43]

Novel biodegradable 2D titanium diselenide nanosheets ($TiSe_2$ NS) were synthesized and applied for enhanced photocatalytic therapies, and photothermal collaborative anticancer phototherapy caused cancer cells to undergo necrosis and apoptosis through the HSP90/JAK3/NF-κB/IKB-α/Caspase-3 pathway.[44a] Park and coworkers described vacuolisation, expanded ER and mitochondria in MH-S murine alveolar macrophages by TiO_2 nanosheets (*ca.* 400 × 400 × 2 nm) and determined that the mechanism of action was induced paraptosis followed by apoptosis.[44b]

In the present era, a considerable number of research reports have emerged on the development of novel drugs, with regard to their cytotoxic profile with improved eco-friendliness and suppressed side effects while modifying the structures of metallodrugs and associated various ligands that have led to versatile metal complexes with remarkable potential as anti-cancer agents. Therefore, parallel to Ti(IV) compounds a few significant different metal compounds have also been described to examine their present and future prospects.[45a] A set of three Pt(II) derivatives associated with dicyclopentadiene (DCP) and dithiocarbamates (DTCs) have been established, which showed greater cytotoxicity (*in vitro* MTT assay) against numerous cancer cell lines, *i.e.* CHL-1, MDA-MB-231, A549 and B16. It is interesting to mention here that on injecting B16 melanoma cells into the right flank of specific-pathogen-free (SPF) mice, Pt-23 at a dose of 8 mg per kg per week inhibited the formation of tumors.[45b] Chiral complexes of Au(III) incorporated with 2-arylpyridine-Au(III)Cl(alkyl-DuPhos) appeared to be anticancer drugs against 4 antagonistic tumor cells *i.e.*, H460, MDA-MB 468, MDA-MB-231 and glioblastoma (BT-33) at micromolar concentrations (IC_{50} 1.3–3.8 μM), and these gold derivatives were compared with the pioneering drug cisplatin (4.16 μM). The findings of the investigation reflected a reduction in tumour growth of 4T1 cancer cells after injecting a 10 mg kg^{-1} body weight dosage into BALB/c mice compared to untreated control mice.[45c] A series of mitochondria-targeting Cu(II) complexes have been reported to assess their cytotoxicity against five cell lines, HL-7702, MGC80-3, T-24, SK-OV-3, and HeLa cells, and normal cells, where they exhibited lower toxicity but greater anti-proliferative efficacy (4.3–5.6 μM) against HeLa cells than cisplatin. Apoptosis was observed from the outcomes of ER stress and cell arrest in the S phase. Tested metal complexes successfully stopped the growth of HeLa xenograft tumours in an *in vivo* mode of analysis.[45d] Very recently, an evaluation of cytotoxicity for thiosemicarbazone ligand supported Ru(II) derivatives towards numerous cancer cell lines, including PANC-1, MDA-MB-231 and MCF7, exhibited extraordinary activity in *in vitro* cytotoxicity, showing superior activity (16.81 to 32.15 μM) over conventional medicines (cisplatin and gemcitabine).[45e] Furthermore, the cytotoxicity of a novel complex of Pd(II) incorporated with the ligand 2,2′-(pyridin2-ylmethylene)bis(5,5-dimethylcyclohexane-1,3-dione) was evaluated against diverse human cancer cells (HCT116, HepG2, MDA-MB-231 and A549) along with normal cells (WI-38), and it demonstrated remarkably lesser toxic effect against normal cells and showed significant activity on HCT116 cells (11 μM).[45f]

The main objective in developing effective and safer anticancer drugs is to damage DNA *via* various binding mechanisms: *e.g.*, hydrophobic binding to the minor groove, intercalation and electrostatic binding. Moreover, intercalation can result in significant changes to the length of the DNA helix, stiffness and unwinding that have powerful impacts on DNA replication and transcription.[46,47] Human serum albumin (HSA, 66.5 kDa) is the most prevalent protein in human plasma; it binds with various ligands associated with metal complexes at various locations, and it plays a vital role in the transport and control over the bioactivity of titanium(IV) derivatives, including cytotoxic drugs. The binding interaction of BSA (75% sequence identity with HSA) with derivatives of titanium(IV) facilitates determination of the affinity constant and primary coordination sites.[48] Bovine serum albumin is a globular protein that appears almost spherical, regulates blood pH, and osmotic pressure as well as being a transporter for various endogenous and exogenous chemicals, including lipids, metals, amino acids, hormones and medication. Details about the distribution, free concentration and metabolic activities of drugs were provided by observations on the interaction between drugs and BSA.[49] The adsorption strength and mobility of binding characteristics are helpful in the study of pharmacokinetics and in designing dose formulation. Such behaviour of drugs is significantly influenced by the discrete surface features and energy of the proteins. The structural resemblance to BSA is frequently employed to estimate the toxicity of HSA.[50] Hexacoordinated titanium(IV) derivatives have also been developed[51–55] along with their demonstrated cytotoxicity, antibacterial and anti-oxidant characteristics, binding patterns with BSA[48] and DNA[56] and catalytic activities for polymerization reactions.[57–59]

Thus, inspired by the spectacular and inspiring multiple pieces of work cited above, we synthesized five new class of homoleptic mononuclear derivatives of titanium(IV) (**TiH_2L^1**–**TiH_2L^5**) coordinated with ONO-sites of ligands and characterized them with relevant spectroscopic tools. Subsequently, BSA, CT-DNA binding interactions, molecular docking and cytotoxicity against HeLa and A549 cell lines were investigated. Since, there are only a few research reports available in closely related fields, the current findings in this article, while encompassing the primary mechanism of titanium(IV) complexes interacting with BSA and CT-DNA, may cause a potential cascade of interest. The cytotoxicity of **TiH_2L^2**–**TiH_2L^4** has been evaluated against HeLa and A549 cell lines by employing an MTT assay. The cell cycle analysis, ROS quantification by DCFH-DA staining assay and Annexin V-APC/PI for apoptosis detection assay were used to find out the apoptosis of HeLa cells.

2. Results and discussion

2.1 Synthesis and structural characterization

The ligand derivatives (H_2L^1–H_2L^5) in this present research work were prepared and purified by established methods.[60] Spectral data (^1H, ^{13}C and FTIR) of these ligands (H_2L^1–H_2L^5) are provided in the ESI (Fig. S1–S6†). Then, a THF (10 mL)

solution of tetraisopropyl titanate (TPT) was refluxed with the ligand concerned (H_2L^1–H_2L^5) in 1 : 2 stoichiometry (Scheme 1) for 24 h to furnish the corresponding titanium(IV) derivative (**TiH_2L^1–TiH_2L^5**). Once completion of the reaction had been assured, excess solvent was driven off at low pressure; then, the resultant crude product was washed thrice with ethyl acetate/*n*-hexane (3 : 7) to obtain the neat form of the final product as a reddish brown solid in remarkable yield (>80%). The structural elucidation of newly developed complexes **TiH_2L^1–TiH_2L^5** was carried out using relevant spectroscopic techniques, such as NMR (^{1}H and ^{13}C), FTIR and HRMS with all spectral data available in Fig. S7–S13.†

2.2 NMR spectra of TiH_2L^1–TiH_2L^5

Proton NMR spectra of complexes **TiH_2L^1–TiH_2L^5** with the disappearance of a couple of free OH protons from the ligands (H_2L^1–H_2L^5) in the range of 10.05 to 15.23 ppm is signature evidence for bond formation between the phenolic oxygen and central metal Ti. Fig. 1 displays the proton NMR spectra of $Ti(OPr^i)_4$, untreated ligands (H_2L^4) and complex **TiH_2L^4** for comparative study, where the methyl and methyne protons of $Ti(OPr^i)_4$ were located from 1.17 to 1.18 ppm and 4.40–4.43 ppm. After complex formation, isopropoxy groups and free OH protons at 15.06 and 10.09 ppm had completely vanished. Further, the imine protons of **TiH_2L^1–TiH_2L^5** were observed as singlet peaks in the range of 8.31–10.42 ppm, and the rest of aromatic protons were found as expected (6.83–8.26 ppm) to authenticate the formation of new complexes. In addition, ^{13}C NMR spectra demonstrated the complete disappearance of isopropxy moieties *i.e.* methyl and methyne carbons at around 21.71–26.42 and 64–70 ppm, respectively. Phenolic carbon (C–O), carbon bonded with nitrogen as single (C–N) and double (C=N) bonds of ligand moieties appeared at 163.82–164.06 ppm, 145.15–150.94 ppm and 151.22–151.25 ppm, respectively. Thus, NMR spectral data strongly verified the successful formation of mononuclear titanium(IV) complexes (**TiH_2L^1–TiH_2L^5**).

2.3 FTIR spectra of TiH_2L^1–TiH_2L^5

The reliable vibrational stretching frequencies of newly developed titanium(IV) complexes **TiH_2L^1–TiH_2L^5** were examined by matching them with the authentic bonding pattern of the relevant free ligands H_2L^1–H_2L^5. Deprotonation of broad OH peaks (3036–3076 cm^{-1}) of the free ligands and generation of corresponding new strong peaks ranging from 432 to 493 cm^{-1} in all the complexes revealed bond formation of Ti–O in respective derivatives (Table S1†).[52] Significant stretching frequencies of C=N and phenolic C–O peaks from the ligand moieties were clearly visible at around 1603 cm^{-1} and 1229 to 1258 cm^{-1}, respectively. Subsequently, Ti–N and Ti–halogen bond stretching frequencies were located at 533–546 cm^{-1} and 735–743 cm^{-1}, respectively. Moreover, these vibrational spectra verified the elimination of all four isopropoxy moieties from $Ti(OPr^i)_4$ by coordination with corresponding ligands to appear as new complexes. The FTIR spectra of **TiH_2L^1–TiH_2L^5** are displayed in Fig. S12.† The FTIR spectra of all the complexes of Ti(IV) displayed stretching frequencies from 533 to 546 cm^{-1} because of the appearance of the new bond Ti–N (of the ligand), emerging as more evidence for the octahedron of Ti(IV) derivatives.[43]

2.4 Photo-physical studies

Absorption and emission spectra of titanium(IV) complexes (**TiH_2L^1–TiH_2L^5**) were measured in a mixture of DMSO and

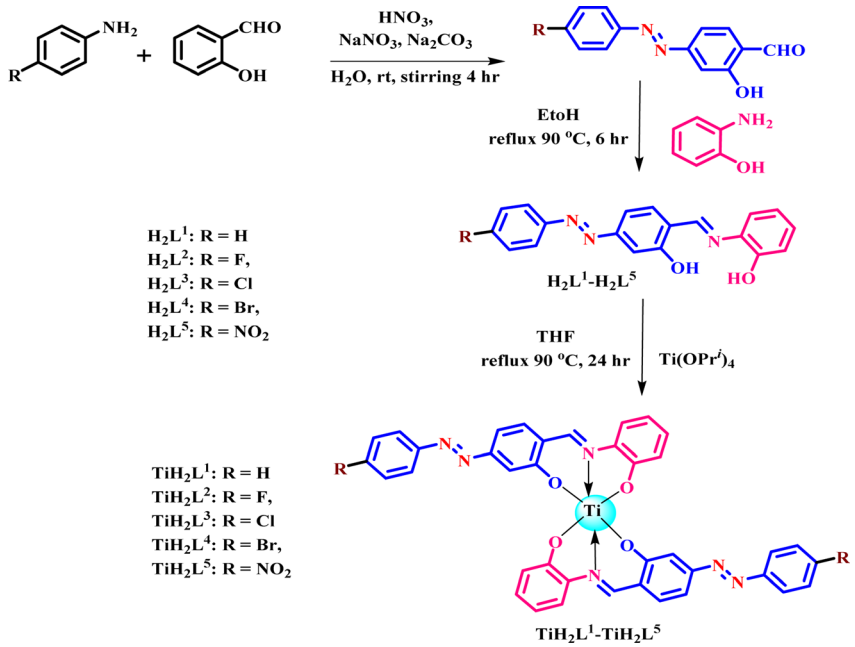

Scheme 1 Sketch of how to obtain ligands (H_2L^1–H_2L^5) and their titanium(IV) derivatives (TiH_2L^1–TiH_2L^5).

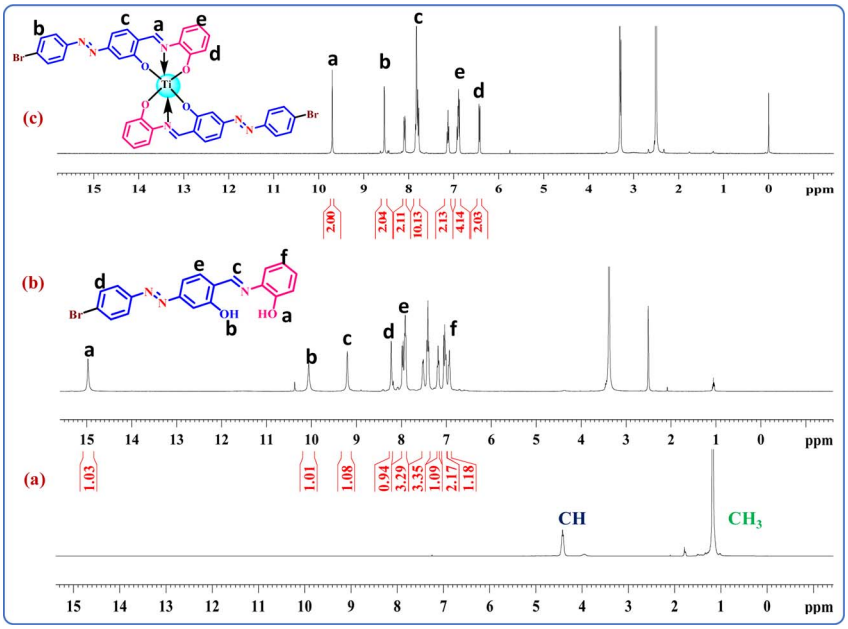

Fig. 1 ^{1}H NMR spectra: (a) $Ti(OPr^i)_4$, (b) H_2L^4 and (c) TiH_2L^4.

water (1 : 1) at 298 K, and the photophysical data are given in Table 1.[61] Fig. S14† shows the absorption spectra of the ligands (H_2L^1–H_2L^5) and newly synthesized titanium(IV) complexes (**TiH_2L^1–TiH_2L^5**). The representative intra-ligand (π–π*) transitions were located at 349–375 nm, and after the formation of metal complexes, these transitions were shifted in the range of 371–470 nm due to metal to ligand charge transfer (MLCT), where the highest absorbance was observed at 470 nm in the nitro-substituted metal complex (**TiH_2L^5**). MLCT peaks underwent a red shift with an increase in the value of the extinction coefficient. Similarly, the emission spectra (MLCT) were also recorded and found to be between 400 and 600 nm. Complex **TiH_2L^5** exhibited strong absorption and emission spectra that were highly intense because of π conjugation due to the availability of a strong electron-withdrawing group (NO_2). The quantum yield of the prepared complexes was calculated using eqn (1) from the emission spectra of the corresponding complexes. UV-visible absorption bands of the derivatives showed a red shift (371–470 nm) due to n–π* transitions (MLCT) while forming new bonds of Ti–O and Ti–N in all five Ti(IV) derivatives because the nitrogen lone pair could also participate in bond formation with the central metal to furnish stability through hexa-coordination.[43,55]

2.5 Stability studies by UV-visible spectroscopy

Potential therapeutic agents should depend on a stable chemical entity present on them. Stability studies of **TiH_2L^1–TiH_2L^5** were investigated by a UV-visible technique. To carry out an investigation of stability, two different media, 10% DMSO/water and 1 mM GSH (glutathione), were considered. The absorbance of samples was recorded at regular intervals such as at 0, 24 and 48 h for 10% DMSO and at 0, 12, 24 and 48 h for GSH, and the relevant findings are exhibited in Fig. S15 and S16,† respectively (Table 1). Derivatives **TiH_2L^1–TiH_2L^5** were found to be stable in the appropriate medium, and their absorption bands displayed only minor variations over the time period of 48 h. These observations suggested that these complexes could make good pharmaceutical candidates for bioassays since they were

Table 1 Photophysical properties, solubility, lipophilicity and conductivity studies of TiH_2L^1–TiH_2L^5

								$\hat{M}^g$ (S m^2 mol^{-1})	
Complexes	$\lambda_{max}{}^a$ (nm)	$\lambda_f{}^b$ (nm)	Stokes shift	OD^c	ε^d (M^{-1} cm^{-1})	$(\Phi^f)^e$	log $P_{o/w}{}^f$	DMSO	10% DMSO
TiH_2L^1	371	422	51	0.51	17 000	0.2349	0.57	6	34
TiH_2L^2	378	430	52	0.53	17 666	0.2243	0.95	7	33
TiH_2L^3	388	441	53	0.57	19 000	0.3080	1.42	7	46
TiH_2L^4	389	427	38	0.50	16 666	0.2294	1.18	6	34
TiH_2L^5	470	554	84	0.76	25 333	0.1620	0.83	6	30

^{a} Absorption maxima. ^{b} Maximum emission wavelength. ^{c} Optical density. ^{d} Extinction coefficient. ^{e} Quantum yield. ^{f} *n*-octanol/water partition coefficients; and. ^{g} Conductance in DMSO and 10% aqueous DMSO (complex concentration 3 × 10^{-5} M).

appreciably stable in the medium used. It is typically believed that substances, which can form aqua complexes in a biological environment and facilitate binding with DNA base pairs through a covalent mechanism of action, damage the DNA structural pattern to inhibit uncontrolled proliferation of cancer cells; thus, these drug molecules could be claimed as potential therapeutic agents. The findings collected from UV-visible examination revealed that the five complexes **TiH_2L^1–TiH_2L^5** possess significant aquatic stability with a mild hypochromic shift in their corresponding absorption bands.

2.6 Solubility, lipophilicity and conductivity

The potential tumor-inhibiting nature and pharmacotherapeutic values of drug molecules are strongly influenced by the lipophilicity and hydrophilicity of the metal complexes. The newly developed titanium(IV) derivatives were fairly soluble in aprotic solvents (DMSO and DMF), but the solubility was moderate to good in protic solvents (H_2O, MeOH, and EtOH), and they were almost insoluble in a hydrocarbon medium. The solubility ranges for each of these derivatives were observed between 4 and 10 mg mL^{-1} in DMSO : DMEM of 1 : 9 (v/v) at 25 ° C. The cellular accumulation and oral bioavailability of drugs were assessed by their lipophilicity. The *n*-octanol/water partition coefficient ($\log P$) is a significant requirement in many *in vitro* pharmaceutical techniques. The partition coefficient of *n*-octanol/water ($\log P_{o/w}$, where $P_{o/w}$ = the octanol/water partition coefficient) was examined by using the shaken flask method. Experimental $\log P_{o/w}$ values of all titanium(IV) derivatives were obtained between 0.83 and 1.42 (Table 1), and plots are made available in Fig. S17.† Chlorine and bromine substituted complexes **TiH_2L^3** and **TiH_2L^4** exhibited pretty high $\log P_{o/w}$ values because of the more lipophilic character of halogens, which appeared to enhance nuclear accumulation.

The descending order of lipophilicity for the derivatives could be expressed as **TiH_2L^3** > **TiH_2L^4** > **TiH_2L^2** > **TiH_2L^5** > **TiH_2L^1**. The molar conductivities of **TiH_2L^1–TiH_2L^5** were found to be in the range of 6 to 7 S m^2 M^{-1} in DMSO. However, in 10% DMSO/water medium, molar conductivities were increased by more than 5 times (30 to 46 S m^2 M^{-1}). This enhancement in conductance could be credited to ionisation and aqua complexation. Further, the cationic behaviour of the titanium(IV) complexes was amplified with increases in the concentrations of GSH and DNA, reflecting the higher cationic properties of titanium(IV) derivatives as a crucial property of drugs to treat cancer cells.

2.7 Density functional theory

Computational studies of the synthesized ligands (H_2L^1–H_2L^5) and their titanium(IV) complexes (**TiH_2L^1–TiH_2L^5**) were carried out by the combined DFT-B3LYP method using Gaussian 09 computational codes. Different quantum-chemical parameters were calculated by applying B3LYP/6-31G**/LanL2DZ ECP methods, such as molecular energy, ESP charges, the energy of frontier molecular orbitals and bandgap. The highly preorganized planar geometries of the ligands (Fig. S18†) and tentative octahedral geometry of **TiH_2L^1–TiH_2L^5** are clearly exhibited (Fig. S19†). The electrostatic potential mapped onto the constant electron density surface for the optimized geometry on the van der Waals surface. This is also very useful in research into molecular structures with their photophysical properties as well as hydrogen bonding interactions in the free ligands and in their titanium(IV) complexes. The maximum negative region, which is the preferred site for electrophilic attack, is indicated by a red colour and the maximum positive region, which is the preferred site for nucleophilic attack, by a blue colour (Fig. S20†). The dipole moments of the free ligands are almost halved after complex formation with titanium. A comparison of the frontier molecular orbitals (FMOs) with the highest occupied molecular orbital (HOMO) and lowest unoccupied molecular orbital (LUMO) with the energy gap between HOMO and LUMO of all the free ligands (Fig. S21†) and their titanium(IV) complexes were calculated and are displayed in Fig. 2 and Table S2.† The ligands exhibit a band gap energy ranging from 3.01 to 2.54 eV, whereas upon coordination with titanium(IV), the band gap shrank in the range of 2.67 to 2.38 eV. Further, the energy gap (ΔE) is an important parameter to characterize the chemical reactivity and kinetic stability of the molecule.[62] A smaller energy gap facilitates easy charge transfer that influences the biological activity of the molecules. The energies of frontier molecular orbitals (E_{HOMO} and E_{LUMO}) and ΔE could be attributed to the eventual charge transfer interaction within the molecule and electronegativity (χ), chemical potential (μ), global hardness (η), global softness (S) and global electrophilicity index (ω) are listed in Table S2.†[63] The importance of these parameters is to measure molecular stability and reactivity. The electrophilicity index is one of the most important quantum chemical parameters in describing the toxicity of various pollutants in terms of their reactivity and site selectivity; the electrophilicity property also quantifies the biological activity for drug–receptor interaction.

TD-DFT calculations of ground-state optimized geometries were performed, and studies of corresponding electronic transitions with their associated orbital contributions were also carried out. The free ligands display two electronic bands, the first appearing in the range from 469.62 to 551.39 nm for weak charge transfer bands, and the second one being observed in the region from 366.04 to 377.94 nm for strong $\pi \rightarrow \pi^*$ transitions (Fig. S22†). Similarly, after complex formation a couple of absorbance bands were again visible as intense bands (395.91 to 417.39 nm) depicting $\pi \rightarrow \pi^*$ transitions, and weak charge transfer bands were detected in the range of 565.94 to 577.05 nm because of ligand to metal charge transfer (LMCT). Interestingly, experimental and predicted absorbance bands were found to be closely comparable, and their characteristic electronic transitions are made available in Table S2.† Moreover, the predicted UV-visible spectra of free ligands and their titanium(IV) complexes are displayed in Fig. S14.†

DFT optimized geometry of the complexes (**TiH_2L^1–TiH_2L^5**) displayed distorted octahedral geometry with characteristic bond lengths of the representative complex **TiH_2L^1** being $O_{1a}\cdots$Ti 1.947, $O_{2b}\cdots$Ti 1.947 and $N_a\cdots$Ti 2.092 (Table S3†). Similarly, the bond angles of the complex **TiH_2L^1** are $O_{1a}\cdots Ti\cdots N_a$ 87.29°, $O_{2a}\cdots Ti\cdots N_a$ 80.63°, $O_{1b}\cdots Ti\cdots N_b$ 89.60° and $O_{2b}\cdots Ti\cdots N_b$

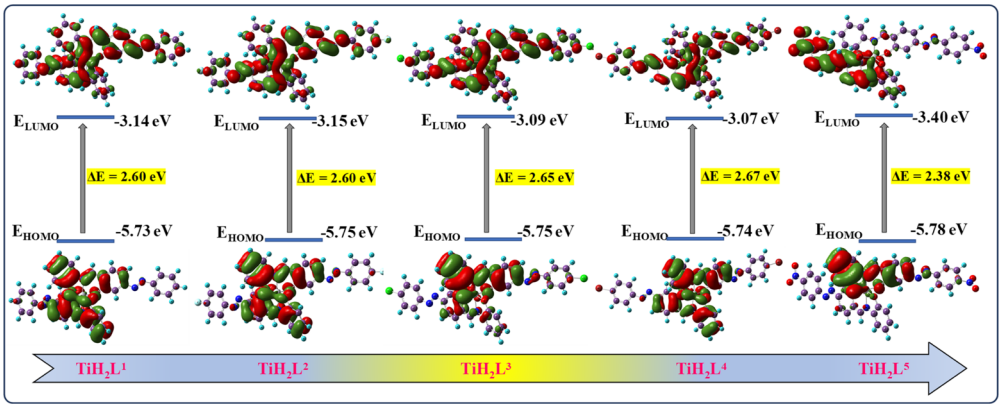

Fig. 2 FMOs of titanium(IV) complexes (TiH_2L1–TiH_2L5) by the DFT/B3LYP method.

79.79°. Though these representative data have been provided here, the entire set of relevant bond lengths (Å) and bond angles (°) corresponding to the octahedral structure of all the derivatives are tabulated in Tables S3 and S4,† respectively.

2.8 DNA binding studies by UV-visible absorption technique

Too develop efficacious chemotherapeutic drugs, it is imperative to investigate how metal complexes interact with DNA. Electronic absorption titration is the most relevant technique that is frequently employed to identify the types of interaction taking place between metal complexes and DNA. Hyperchromism and hypochromism are two common spectral features of electronic titrations of complexes with CT-DNA. Drug molecules can interact with DNA in three major different non-covalent ways: (A) intercalation, (B) partial intercalation and (C) groove binding; and these could be supported by interactions between hydrogen atoms, electrostatic charges and hydrophobic bonds. Electronic transitions are induced by DNA base pairs, such as purine (adenine and guanine) and pyrimidine (cytosine and thymine) base analogues. Derivatives **TiH_2L^1–TiH_2L^5** exhibited distinct absorbance bands at 256–262 and 362–404 nm due to intraligand $\pi \rightarrow \pi^*$ transitions and MLCT, respectively. During the addition of DNA (5 to 50 μM) to **TiH_2L^1–TiH_2L^5**, hyperchromic shifts (256–262 nm) were observed, and hypochromic shifts (362–404 nm) were also noticed (Fig. S23†), which, along with formation of an isosbestic point, indicate the existence of intercalative and covalent modes of interaction between the DNA and complexes. Hypochromism and isosbestic point are representative for complexes binding with DNA base pairs in an intercalative manner, which is undoubtedly recorded in the present investigation.[40,56,61] Conversely, hyperchromism is the result of cleavage of the secondary DNA structure as groove binding, and it does not have any scope herein. It is reasonable to predict that the positively charged titanium(IV) moiety might have disturbed the negatively charged phosphate group of CT-DNA. External contact (electrostatic binding), groove binding, covalent binding or partial untwisting of the DNA helix structure facilitate the incorporation of additional DNA bases into the drug molecules and might cause significant hyperchromism.[61,64] The intrinsic binding constants (K_b) for **TiH_2L^1–TiH_2L^5** were found with eqn (2) $[DNA]/(\varepsilon_a - \varepsilon_f)$ *vs.* [DNA], and the plots are displayed in Fig. S24† (Table 2). The intrinsic binding constants of **TiH_2L^1**, **TiH_2L^2**, **TiH_2L^3**, **TiH_2L^4**, **TiH_2L^5** were found to be 1.12×10^5 M^{-1}, 2.27×10^5 M^{-1}, 1.11×10^5 M^{-1}, 1.07×10^5 M^{-1} and 0.7×10^5 M^{-1}, respectively.

2.9 EtBr displacement assay

Ethidium bromide (EtBr) was used as an efficient fluorophore in fluorescence spectroscopy to examine the competitive intercalative binding of **TiH_2L^1–TiH_2L^5** with DNA.[61,65,66] The cationic dye and planar nature of EtBr itself displayed weak emission intensity in the buffer, but after binding with DNA it exhibited a strong emission peak due to intercalation between EtBr and DNA base pairs to form DNA-EtBr adducts. Subsequently, on addition of **TiH_2L^1–TiH_2L^5** into the DNA-EtBr adducts, smaller to moderate fluorescence quenching intensities were observed that were indicative of the displacement of EtBr by **TiH_2L^1–TiH_2L^5** from the double helix of DNA. This is a prime illustration of the DNA double helix being modified by **TiH_2L^1–TiH_2L^5**. CT-DNA-EtBr adducts were excited at 480 nm, and the emission peak appeared at around 596 nm. The primary fluorescent intensity of the DNA-EtBr adducts was observed at around 596 nm, and it was gradually lowered (hypochromic patterns) to 50 nm due to the addition of the derivatives **TiH_2L^1–TiH_2L^5** (0–50 μM), indicating intercalation of DNA with the respective complexes (Fig. S25†). As per reports, an increase in the fluorescence intensities of the complexes while titrating with CT-DNA indicates groove binding, but in present studies, a remarkable decreasing trend in the intensity of fluorescence is observed during the addition of a greater concentration of complexes into CT-DNA. Such findings clearly stand for intercalation binding, and it was able to replace the intercalation-bound EtBr dye from the double-stranded DNA helix.[26,67] The Stern–Volmer quenching constant (K_{SV}) was calculated with eqn (4), and the data obtained for **TiH_2L^1–TiH_2L^5** are displayed in Table 2, and the plots are exhibited in Fig. S26.† Scatchard plots for complexes **TiH_2L^1–TiH_2L^5** are displayed in Fig. S27,† and complex **TiH_2L^3** reflected a higher number of binding sites (1.9) than those of the other derivatives. Binding parameters, such as Stern–Volmer quenching constant, binding

Table 2 Binding parameters for the interaction of CT-DNA with TiH_2L^1–TiH_2L^5

Complex	λ_{max}	Change in absorbance	Δ_ε[a] (%)	K_b[b] (10^5 M^{-1})	K_{sv}[c] (10^6 M^{-1})	n[d]	K_{app}[e] (10^6 M^{-1})
TiH_2L^1	370	Hypochromism	51	1.12	0.009	1.09	0.73
TiH_2L^2	362	Hypochromism	44	2.27	0.056	0.85	1.66
TiH_2L^3	371	Hypochromism	46	1.11	0.016	1.19	1.71
TiH_2L^4	365	Hypochromism	58	1.07	0.041	0.85	1.54
TiH_2L^5	404	Hypochromism	37	0.7	0.218	1.16	1.53

[a] % change in hypochromism (Δ_ε). [b] Intrinsic DNA binding constant (K_b) from UV–visible absorption titration. [c] Stern–Volmer quenching constant (K_{SV}). [d] Binding sites (n); and. [e] Apparent DNA binding constant of DNA from EtBr displacement (K_{app}).

rate constant and binding sites for the interaction of DNA with TiH_2L^1–TiH_2L^5, are tabulated in Table 2.

2.10 Relative viscosity method

Viscosity measurement is highly sensitive, hydrodynamic and one of the most reliable techniques for determining the binding mode of a drug with CT-DNA in solution.[26] Typical intercalation binding requires the separation of neighbouring base pairs to allow binding of drug molecules into the DNA double helix, resulting in an increase in DNA viscosity and contour length.[26,67] Viscosity experiments with CT-DNA were used to find out the binding interactions of CT-DNA with various concentrations of TiH_2L^1–TiH_2L^5. Intermolecular interactions between the complexes and CT-DNA cause a change in the relative viscosity of CT-DNA.[61] The findings are revealed by plotting relative viscosity $(\eta/\eta_0)^{1/3}$ *vs.* the molar ratio of titanium(IV) derivatives to DNA, as displayed in Fig. S28.† As predicted by the intercalative interaction pattern, the relative viscosity of CT-DNA was gradually elevated on an increase in the concentration of the complexes, and a similar pattern was also visible for EtBr. After accommodating TiH_2L^1–TiH_2L^5 into CT-DNA, the resultant separation of the base pairs of CT-DNA elongated the double helix of CT-DNA. The binding pattern of the metal complexes might twist the DNA structure because of partial or nonclassical binding and change the viscosity followed by the length of DNA. It is worthwhile mentioning here that present investigations reflect a remarkable increase in DNA viscosity based on the intercalation mode of binding. Though groove binders do not change the axial length of DNA upon binding, and they also do not influence the relative viscosity of DNA, a tiny rise in the relative viscosity could also be considered a sign of groove binding.

2.11 ^{1}H NMR spectroscopy of CT-DNA-TiH_2L^3 system

A crucial method for examining and comprehending at the molecular level how a small drug molecule binds with its target receptor like CT-DNA is the nuclear magnetic resonance (NMR) technique. Specifically, ^{1}H NMR is the most widely used atomic nuclei method for DNA binding research because it does not have limitations on molecular size or a requirement of isotope-labelling.[67] Two important features of NMR spectra that are examined during drug–DNA interactions are changes in line widths and chemical shifts. Proton NMR signals could be easily distinguished among the three different types of interaction mode. Type I binding: intercalating molecules between DNA base pairs with drugs lead to the total line broadening of the chemical shift. Type II binding: regarding a partially intercalated molecule, line broadening or upfield chemical shift was found in the signal related to the drug-bound DNA because the molecular tumbling in the complex with CT-DNA was weakly restricted or occurrence of delayed exchange between the different binding sites of DNA in the free state of the molecule. Type III binding: molecules bound to DNA were not displayed, and there was no line broadening or upfield chemical shift of the ^{1}H NMR signal referring to groove binding.[26,67]

^{1}H NMR measurements (298 K, 400 MHz) were performed to investigate the interaction mode when CT-DNA is bound with the TiH_2L^3 system. ^{1}H NMR spectra of TiH_2L^3 in the presence and absence of CT-DNA are displayed in Fig. 3. A close comparison of Fig. 3a and b reveals evident line broadening of H-a, b, c and d peaks after treatment with CT-DNA, and it is representative of the fact that the addition of CT-DNA influences the microenvironment of TiH_2L^3 protons. Table S5† displays the negligible upfield shift of proton resonances of a, b, c and d in the presence of CT-DNA, possibly reflecting π–π stacking interactions between TiH_2L^3 and the base pairs of CT-DNA. The electron density around these protons after CT-DNA has bound with TiH_2L^3 has increased due to magnetic shielding effects. Thus, ^{1}H NMR spectra evidently demonstrate that in the presence of CT-DNA, extensive broadening of different peaks was observed, indicating binding of TiH_2L^3 with DNA *via* the intercalation mode.

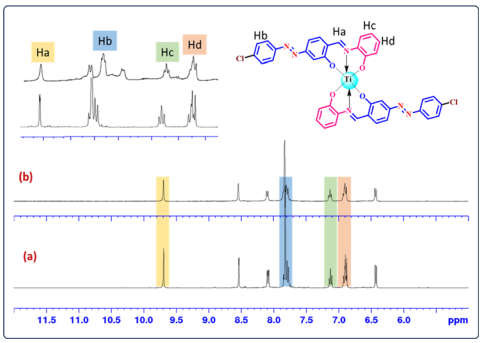

Fig. 3 ^{1}H NMR spectra of TiH_2L^3 in the absence (a) and presence (b) of CT-DNA in DMSO-d_6 : D_2O (2 : 3) at 298 K.

2.12 BSA protein binding

The fluorescence of BSA is mostly caused by the presence of amino acids such as tyrosine, phenylalanine and tryptophan. Among these, tryptophan plays a significant role in the intrinsic fluorescence of BSA. To investigate the nature of the binding interaction of BSA with **TiH_2L^1–TiH_2L^5**, electronic absorbance (Fig. S29†) and fluorescence (Fig. S30†) titration data were recorded with a constant concentration of BSA against various concentrations of **TiH_2L^1–TiH_2L^5**. Initially, the binding interaction of BSA was studied by UV-visible titration, and the excitation peak of BSA observed at 280 nm reflected red shifts in the range of 344–404 nm (Fig. S29†) because of interactions with **TiH_2L^1–TiH_2L^5**. Regarding fluorescence titration, a BSA excitation peak was found localised at 280 nm, but the emission intensity (344 λ_{em}) exhibited a descending pattern on the addition of **TiH_2L^1–TiH_2L^5** (2.5–20 μM) (Fig. S30†), due to deformation of the morphology of the protein. Thus, a lowering of quenching intensity demonstrated the type of interaction between BSA and quencher molecules (**TiH_2L^1–TiH_2L^5**) *via* static superseding dynamic quenching.

Collisional or dynamic quenching occurs during interaction between the quencher and excited state of the BSA fluorophore to make it inactive. Static quenching takes place when non-fluorescent ground-state complexes interact with BSA.[65,68] Initially, it was considered that quenching of fluorescence predominantly involves a static mechanism. The fluorescence quenching constant (K_{BSA}) was described by the Stern–Volmer eqn (5), as highlighted in Fig. S31,† where plots are drawn between F_0/F and the concentration of quencher (**TiH_2L^1–TiH_2L^5**), which undoubtedly exhibited the appearance of a straight line that confirmed static quenching. Based on the quenching rate constant, the number of binding sites were calculated (eqn (6)) from the Scatchard plots, as revealed in Fig. S32.† All the titanium(IV) complexes (**TiH_2L^1–TiH_2L^5**) displayed a strong binding tendency with BSA, which is essential for the transport of protein-bound complexes in biological systems. Our findings support the suitable intrinsic fluorescence static quenching process developed herein that occurs when BSA interacts with **TiH_2L^1–TiH_2L^5**.

The quenching rate constant (K_q) values for the interaction of BSA with individual **TiH_2L^1**, **TiH_2L^2**, **TiH_2L^3**, **TiH_2L^4** and **TiH_2L^5** are found to be 0.7×10^{13} M^{-1}, 3.0×10^{13} M^{-1}, 4.2×10^{13} M^{-1}, 3.4×10^{13} M^{-1} and 4.5×10^{13} M^{-1}, respectively. Though **TiH_2L^3** and **TiH_2L^5** exhibited higher quenching rate constants ($4.2–4.5 \times 10^{13}$ M^{-1}), **TiH_2L^3** displayed the highest number of binding sites, *i.e.* 1.4, with a quenching constant of 4.2×10^{13} M^{-1}, which exceeded the maximum scatter collision quenching constant of BSA (2×10^{10} M^{-1}) resulting from the linkage with static quenching. The UV-visible, fluorescence quenching, Scatchard and Stern–Volmer plots of BSA interaction with **TiH_2L^3** are exhibited in Fig. 4. These complexes appear to be highly effective at treating cancer cells because of their strong association with BSA, which circumvents GSH-mediated drug resistance. The binding parameter values of BSA, such as quenching rate constant, Stern–Volmer quenching constant, binding constant and binding sites for the interaction of BSA with **TiH_2L^1–TiH_2L^5** are given in Table 3.

2.13 CD spectral analysis

The CD spectral technique is an extremely suitable tool to identify any modification in the secondary structures of DNA, proteins and in polypeptides caused by interacting molecules. More precisely, CD analysis illustrates the distortion occurring

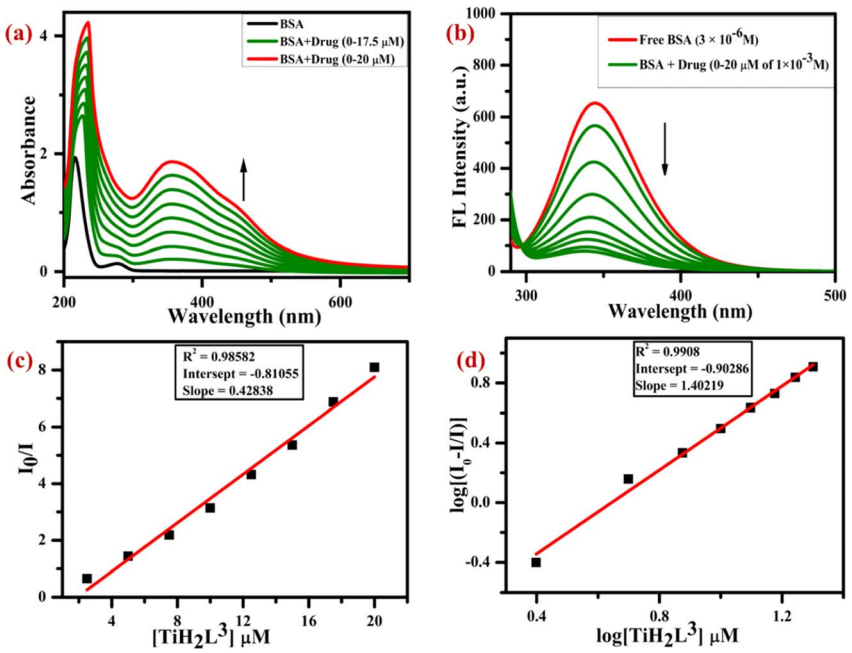

Fig. 4 (a) BSA binding plots of TiH_2L^3 by UV-visible method. (b) Fluorescence quenching plot of BSA with TiH_2L^3. (c) Stern–Volmer plots of I_0/I *vs.* [TiH_2L^3]. (d) Scatchard plot of $\log([I_0 - I]/I)$ *vs.* $\log[TiH_2L^3]$.

Table 3 Binding parameters for the interaction of BSA with TiH_2L^1–TiH_2L^5

Complex	K_{BSA}[a] (10^6 M^{-1})	K_q[b] (10^{14} M^{-1} s^{-1})	K_b[c] (10^5 M^{-1})	n[d]
TiH_2L^1	0.0759	0.0759	0.718	0.35
TiH_2L^2	0.30504	0.30504	0.3421	0.93
TiH_2L^3	0.42838	0.42838	0.1230	1.4
TiH_2L^4	0.34748	0.34748	0.2194	1.1
TiH_2L^5	0.4564	0.4564	0.2521	1.14

[a] Stern–Volmer quenching constant (K_{BSA}). [b] Quenching rate constant (K_q). [c] Binding constant with BSA (K_b); and. [d] Number of binding sites (n).

in the DNA backbone during binding with any probe. There is a strong correlation between variations detected by CD signals of DNA and DNA modifications concerned. After getting remarkable results from UV-visible and spectrofluorometric investigation of CT-DNA and BSA after treatment with **TiH_2L^2–TiH_2L^4**, their conformational changes were further confirmed by CD spectral analysis. The typical CD spectrum of CT-DNA has a negative band at 244 nm and a positive band at 273 nm, due to the right-handed B-form, which are correlated with the helical structure and π–π base stacking, respectively.[65] An investigation based on the interaction, decreasing the intensity of the positive band and negative band, found a minor upsurge with a blue shift of 4–10 nm and 2–5 nm in wavelength, respectively (Fig. 5a). These findings imply that at higher concentration (50 μM) of **TiH_2L^2–TiH_2L^4**, DNA binds with the complexes through an intercalative mechanism with significant conformational changes or destabilization of CT-DNA helicity.

There are several intramolecular and intermolecular forces that are elaborate secondary and tertiary structural conformations of the proteins that might be affected by interaction with drug molecules. BSA regions such as disulfide bonds (weak wide absorption bands at 320 nm), aromatic amino acid side chains (260–320 nm) and peptide bonds (>240 nm) were taken into consideration as the protein regions of interest.[69] The representative CD spectrum of BSA exhibited a pair of negative bands at 209 nm and 222 nm wavelength. After treatment with elevated concentrations of **TiH_2L^2–TiH_2L^4** (20 μM), peaks at 208 nm and 222 nm were red shifted around 230 nm because of n–π* transitions of the α-helix from the peptide bond.[65,69] The characteristic helical composition of BSA abruptly vanished and was drastically shifted to longer wavelength due to interaction with metal complexes. This is shown in Fig. 5b, which reveals the CD spectra of BSA alone as well as in the presence of **TiH_2L^2–TiH_2L^4**. As mentioned above, **TiH_2L^2–TiH_2L^4** had an influence on concomitant secondary structural conformational changes in the helicity of BSA through an intercalation mechanism. CD spectra of CT-DNA exhibit 'nominal to no change' with regard to minor groove binding and electrostatic binding, whereas intercalation binding should undoubtedly be considered in the remarkable alteration in positive and negative bands of DNA and that is the finding in the present investigation.[26,67]

2.14 Molecular docking studies

The synthesized derivatives **TiH_2L^1–TiH_2L^5** were subjected to molecular docking investigation by Autodock 4.2, covering the Lamarckian Genetic Algorithm (LGA) to compute the binding affinities of possible conformers. A molecular docking study is an important way to predict the binding interaction and molecular mechanism between drugs and the active sites of a receptor. An appropriate orientation of the complexes has been predicted relative to DNA and BSA for their geometric and energetic conformation with the respective binding sites. In the present work, molecular modelling for **TiH_2L^1–TiH_2L^5** was carried out with the DNA duplex comprising the d(CpGpCpGpApApTpTpCpGpCpG) dodecamer sequence.[70,71] To reinforce experimental protein–complex interactions, molecular docking of **TiH_2L^1–TiH_2L^5** was conducted by procuring the crystallographic structure of BSA. According to a detailed review of the literature, two key binding sites in BSA are in the proximal areas of Trp134 and Trp213, where Trp213 is part of the hydrophobic site, and Trp134 is positioned at the surface of the hydrophilic region. The docking energy clearly illustrated that all of the synthesized titanium(IV) derivatives filled the putative binding region of BSA (Fig. 6). In this respect, **TiH_2L^4** and **TiH_2L^5** were observed to have the highest docking scores: −8.54 kcal mol^{-1} and −7.51 kcal mol^{-1}, respectively. As discussed above, both the complexes revealed hydrogen bonding (3.19 Å) with LEU282, while there was further hydrogen bonding (2.79 Å) with GLU291 residues.

An assessment of each docked molecule was computed by screening scoring functions (Table S6†), which serve as testimony to how well the complexes are bound within the intercalation of CT-DNA (Fig. 7). The negative values associated with

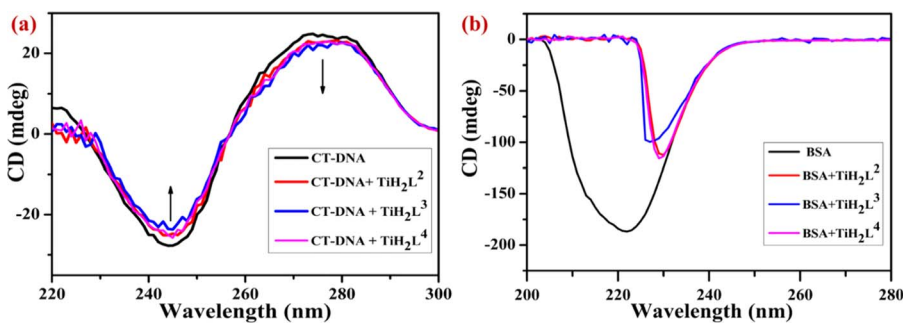

Fig. 5 Circular dichroism spectra: (a) CT-DNA treated with TiH_2L^2–TiH_2L^4 and (b) BSA treated with TiH_2L^2–TiH_2L^4.

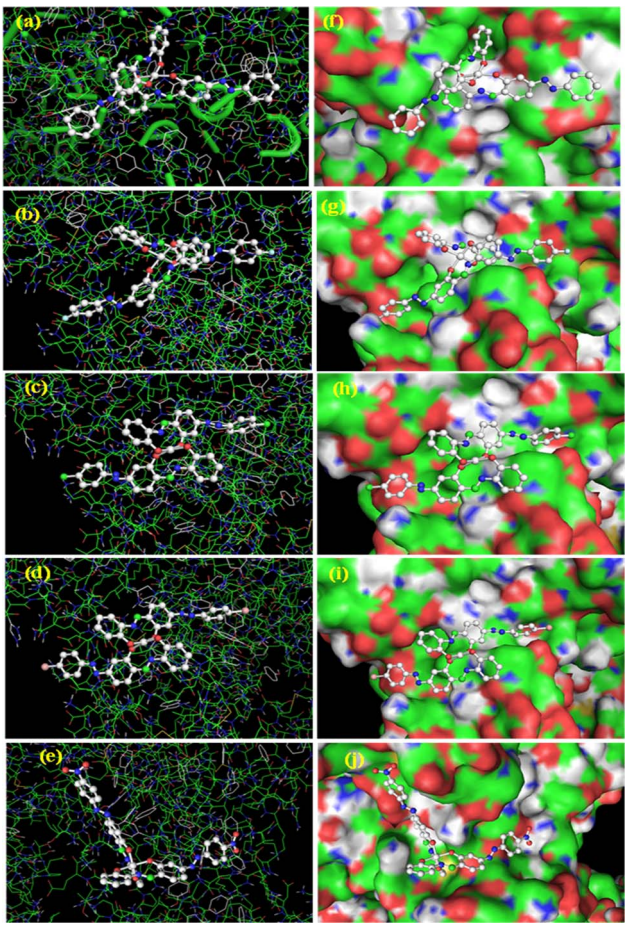

Fig. 6 Optimum posture for interaction of BSA with TiH_2L^1–TiH_2L^5: (a) TiH_2L^1, (b) TiH_2L^2, (c) TiH_2L^3, (d) TiH_2L^4 and (e) TiH_2L^5 and 3D surface binding of TiH_2L^1–TiH_2L^5 with BSA: (f) TiH_2L^1, (g) TiH_2L^2, (h) TiH_2L^3, (i) TiH_2L^4 and (j) TiH_2L^5.

the compounds indicate appropriate binding with DNA. In this regard, $\mathbf{TiH_2L^4}$ and $\mathbf{TiH_2L^5}$ were selected as highly active owing to their highest docking scores: −11.27 kcal mol^{-1} and −11.37 kcal mol^{-1}, respectively. $\mathbf{TiH_2L^2}$ and $\mathbf{TiH_2L^5}$ exhibited one hydrogen bond (3.06 Å) with DT8 and two hydrogen bonds (3.33 and 3.10 Å) with DT8 and DA18, respectively. The reported spectral and other experimental data are consistent with the *in silico* investigation.

2.15 Anti-inflammatory activities

The anti-inflammatory (*in vitro*) activities of $\mathbf{TiH_2L^1}$–$\mathbf{TiH_2L^5}$ with diverse concentrations (50–250 μg mL^{-1}) were examined by employing a BSA denaturation method.[72] A UV-vis spectrophotometer was used to record changes in absorbance of test solutions at 660 nm during the experiments. The effect of anti-inflammation was calculated from the percentage inhibition where diclofenac sodium was taken as a reference standard that displayed concentration-dependant inhibition of 78% at 250 μg mL^{-1}, whereas individual derivatives $\mathbf{TiH_2L^1}$–$\mathbf{TiH_2L^5}$ exhibited 49%, 56%, 68%, 54% and 38%, respectively. The ESI (Fig. S33†) include information on the percentage of $\mathbf{TiH_2L^1}$–$\mathbf{TiH_2L^5}$ that denatures (BSA) inhibition. Complex $\mathbf{TiH_2L^3}$ displayed similar activity for standard diclofenac sodium compared with the other derivatives. The rates of anti-inflammatory activities were found in decreasing order to be $\mathbf{TiH_2L^3}$ > $\mathbf{TiH_2L^2}$ > $\mathbf{TiH_2L^4}$ > $\mathbf{TiH_2L^1}$ > $\mathbf{TiH_2L^5}$.

2.16 *In vitro* cytotoxicity

The anti-proliferative activities of halogen-substituted complexes $\mathbf{TiH_2L^2}$–$\mathbf{TiH_2L^4}$ were further evaluated on HeLa and A549 cell lines by an MTT (methylthiazolyldiphenyl-tetrazolium) assay, as previously described. 96-well plates with cancer cell lines and test samples ($\mathbf{TiH_2L^2}$–$\mathbf{TiH_2L^4}$) in various concentrations (12.5–100 μg mL^{-1}) were incubated at 37 °C for 24 h. The percentage cell viability of the cell lines is influenced by the concentration of corresponding derivatives (electron-withdrawing or electron-donating substituents). Fig. S34a and e† reveal control cell lines of HeLa and A549 cells without treatment with the test samples, but images obtained after treatment with $\mathbf{TiH_2L^2}$–$\mathbf{TiH_2L^4}$ in 100 μg mL^{-1} concentrations are highlighted in Fig. S34b–d for HeLa and Fig. S34f–h† for A549 cells.

The highest concentration (100 μg mL^{-1}) of test samples ($\mathbf{TiH_2L^2}$–$\mathbf{TiH_2L^4}$) displayed the maximum cell inhibition of HeLa and A549 cells compared to the lowest concentration

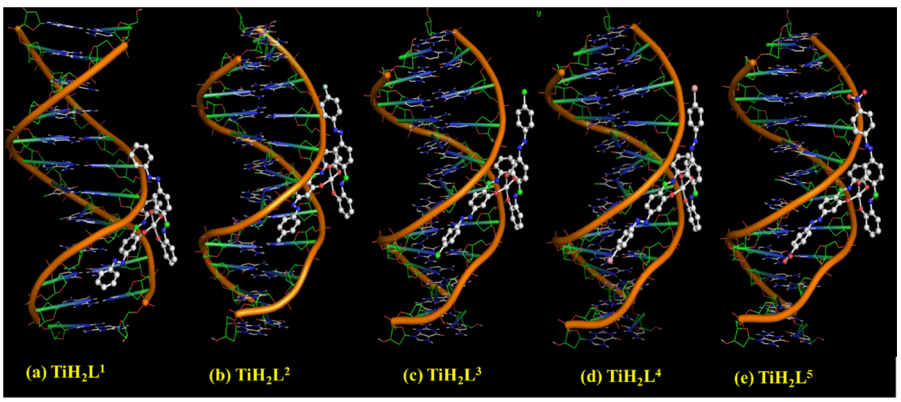

Fig. 7 Optimum posture for molecular docking on CT-DNA with TiH_2L^1–TiH_2L^5.

(12.5 g mL^{-1}). The cells were observed through microscopic studies, showing spherical nonviable cells (dead) in red circles and irregular shaped live cells displayed as blue circles (Fig. S34†). The IC_{50} (half maximal inhibitory concentration) values of TiH_2L^2–TiH_2L^4 were found to be 28.8, 14.7 and 31.2 g mL^{-1} for the HeLa cell line and 52.4, 32.9 and 67.78 μg mL^{-1} for A549 cells, respectively. Fig. 8a and b exhibit the concentrations of test samples *vs.* cell inhibition (%) on HeLa and A549 cells, respectively. Among these derivatives, complex TiH_2L^3 exhibited significant cytotoxicity on HeLa and A549 cell lines, ranging from 14.7 μg mL^{-1} to 32.9 μg mL^{-1}. These changes are due to the most sterically hindered molecules with an electron-withdrawing halogen (Cl) substituted in the *para*-position in the ligands. The electron-withdrawing groups (Cl, Br, and F) substituted on the *para*-position enable them to be more active, whereas *ortho*-positioned halo groups are shown to be less active.[37,39] This could be explained by the cumulative impact of steric groups, which most frequently exhibit greater efficiency, but this could not be generalised due to the specific structures of the molecules concerned.[54,73] The derivatives TiH_2L^2–TiH_2L^4 demonstrate remarkable stability and solubility, but these were likely to be the limiting factors for either the inactivity or diminishing activity of the complexes that were produced in response to HeLa and A549 cells.

2.17 Fluorescence image studies

After observing the remarkable cytotoxicity of complex TiH_2L^3 by MTT assay, we moved ahead towards an investigation of cellular bio-imaging of treated HeLa cells. Cellular imaging is one of the most crucial techniques in biology and medicine and an essential approach for cellular analysis. It is further employed for therapeutic uptake in cells, particularly for determination of the morphology in normal tumour cells, early and late apoptotic cells and necrotic cells. Controlled HeLa cells are marked by crescent-shaped or granular yellow-green acridine orange nuclear staining, as highlighted in Fig. 8c. Late-stage apoptotic cells are indicated with concentrated and asymmetrically localized orange nuclear ethidium bromide staining, as appeared after the treatment of HeLa cells with TiH_2L^3 (Fig. 8d). The number of necrotic cells increased and edges of these cells were found to fluoresce irregularly with orange-red appearance at their periphery. It is easy to see that the conjugate has accumulated in the cytoplasm and nucleus. The above-mentioned findings reveal that malignant HeLa cells uptake TiH_2L^3 more readily, and we recommend that this compound could be employed for the detection of cancer cells and deep tissue imaging.

2.18 Structure–activity relationship (SAR)

SAR signifies that the *para* position of the ligand moieties substituted with electron-withdrawing groups such as fluoro, chloro and bromo (derivatives TiH_2L^2, TiH_2L^3 and TiH_2L^4, respectively) exhibited remarkable cytotoxic profiles in tested cancer cell lines.[34–36] These lipophilic, interchangeable ligands enable the rapid exchange of ligands and might allow a coordinated interaction with biomolecules. Under close comparison, mononuclear complexes were found suitable for DNA intercalation because of their planar aromatic moieties.[32,46] A central

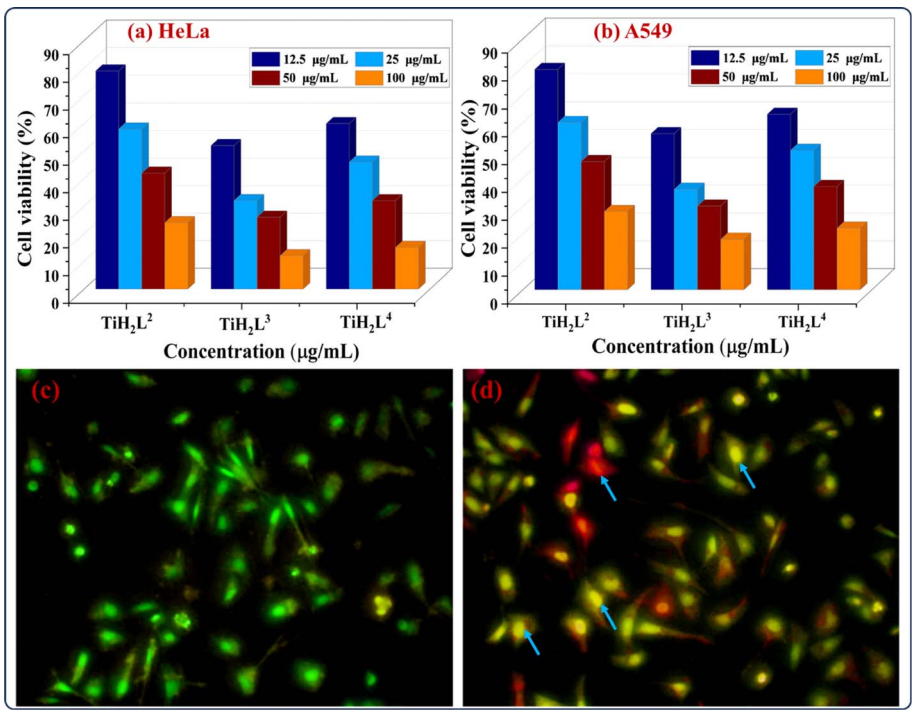

Fig. 8 Bar graph demonstration of the cytotoxicity (IC_{50} value) of TiH_2L^2–TiH_2L^4 from an MTT assay against (a) HeLa and (b) A549 cancer cell lines. Acridine orange fluorescence and bright field images: (c) live HeLa cells denoted as a green nucleus and (d) treated with TiH_2L^3 and late apoptotic cells displayed as condensed and fragmented orange chromatin.

positive ion (Ti^{4+}) facilitates induced apoptosis, destruction of DNA replication followed by protein synthesis, nucleus, mitochondria targeting and intercalation with the negatively charged phosphate backbone of DNA base pairs (Fig. 9). The extended Ph-ring system improved the hydrophobicity, showing π–π interaction with CT-DNA to boost DNA intercalation. A prolonged π-electronic system magnifies fluorescent features for cellular tracking. Among these derivatives, **TiH_2L^3** exhibited significant selectivity against HeLa and A549 cell lines due to its significant cell permeability ($\log p = 1.42$) and DNA binding sites (1.19). A careful analysis of the cytotoxicity of **TiH_2L^2**–**TiH_2L^4** reveals that fluorine and chlorine substituted complexes (**TiH_2L^2** and **TiH_2L^3**) demonstrated almost the same activity towards HeLa and A549 cell lines, but the decrease in the interaction of charged groups of CT-DNA (CO–NH– and –SO_2–NH–) could be attributed to a steric effect.[42]

2.19 Cell cycle analysis by employing flow cytometry

After the stages of growth and DNA replication, interphase (G_1 + S + G_2), nuclear division (mitosis) and cell division (cytokinesis) take place. Three sub-phases are separated out of the interphase. Cell growth, RNA and protein synthesis occur in the G_1 sub-phase. In the next phase, DNA synthesis occurs in the S sub-phase followed by the G_2 phase where cells continue to grow and produce fresh proteins required for cell division. Propidium iodide (PI) is utilised as a DNA intercalating dye that exhibits strong fluorescence upon binding with DNA and could be used to investigate the effect of anti-cancer titanium agents on the cell cycle. The amount of excited PI fluorescence that a single cell contains is directly correlated with its DNA content. The DNA content of population's cells could be put into a histogram to determine the percentage of the cells in each phase of the cell cycle and ways that test compounds disrupt the cell cycle.[19,25]

The cell cycle is a critical process for the normal proliferation of any cell. Numerous drugs work by targeting DNA/specific proteins to block the cells from progressing from one stage of the cycle to another stage of the cycle, resulting in cell cycle arrest.[74] Cell cycle arrest prevents cancer cells from developing into tumors and prevents metastasis. About 38.86% of cells in the control well were in the G_1 phase, followed by the S phase (17.08%) and G_2/M phase with 16.09% cells (Fig. 10). After treatment with an IC_{50} concentration of **TiH_2L^2** compound, the G_1 phase of HeLa decreased to 15.01% followed by the S phase (10.91%) and further the G_2/M phase with 16.23% cells. Similarly, with regard to an IC_{50} dose of **TiH_2L^3**, the G_1 phase of HeLa was reduced to 16.24% followed by the S phase (14.61%) and G_2/M phase (14.90%). Subsequently, the G_1 phase of HeLa was diminished to 14.68% followed by the S phase (14.33%), but the G_2/M phase was slightly elevated with 18.74% cells after treatment with an IC_{50} dose of **TiH_2L^4**. The above-discussed observations from the cell cycle analysis of HeLa cancer cells treated with **TiH_2L^2**–**TiH_2L^4** (Fig. 10), indicate that the titanium(IV) derivatives **TiH_2L^2**–**TiH_2L^4** were effective against HeLa cancer cells and were capable of causing cell cycle arrest in the G_1 phase of the cell cycle.[31]

2.20 Detection of ROS generation by flow cytometry

Reactive oxygen species (ROS) and free radicals play essential roles in the transmission of cell signals and other physiological functions, such as apoptosis, cell proliferation and survival. ROS contain numerous free radicals and reactive molecules, *e.g.* hydrogen peroxide (H_2O_2), hydroxyl radical ($HO^{\bullet}$) and superoxide anion (O_2^{-}), and these radicals are formed in an electron transport chain as byproducts. Conversely, disproportionate ROS levels may interfere with normal biological processes and lead to cellular imbalance in redox reactions, eventually causing damage to DNA, cell membranes and proteins. This situation is known as the cause of oxidative stress, which in turn could lead to the development of a variety of diseases. If they are not controlled, they can react indiscriminately with the molecules in their biological environment. The basis of ROS-inducing strategies is the ability to kill cancer cells by raising the ROS level above the cytotoxic threshold. A greater ROS level leads to disruption of redox homeostasis that is lethal to cancer cells and, eventually,

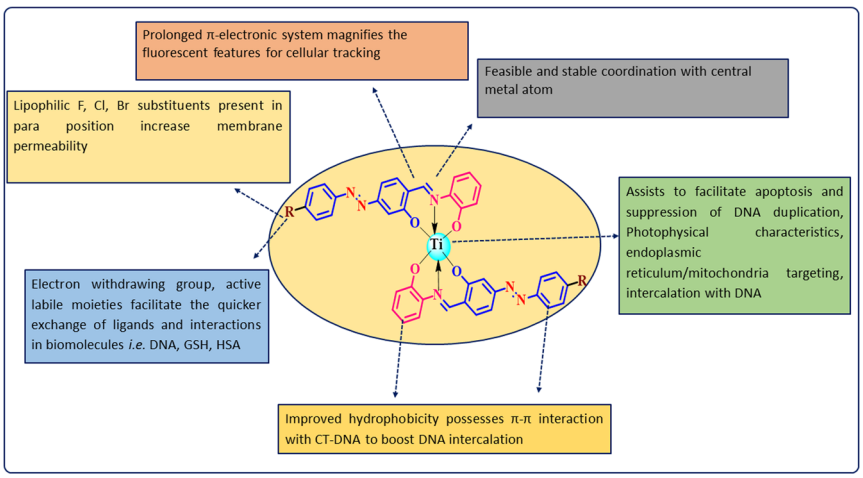

Fig. 9 SAR studies for titanium(IV) derivatives.

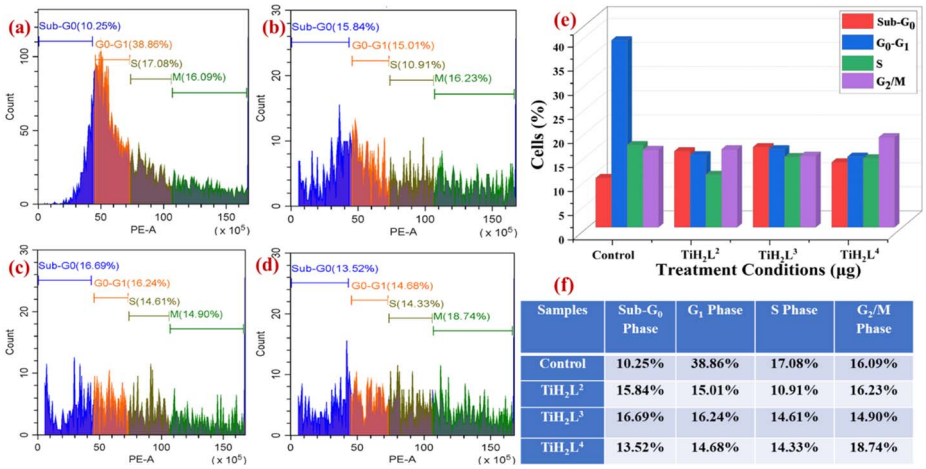

(f)

Samples	Sub-G_0 Phase	G_1 Phase	S Phase	G_2/M Phase
Control	10.25%	38.86%	17.08%	16.09%
TiH_2L^2	15.84%	15.01%	10.91%	16.23%
TiH_2L^3	16.69%	16.24%	14.61%	14.90%
TiH_2L^4	13.52%	14.68%	14.33%	18.74%

Fig. 10 Cell cycle analysis of HeLa cell line by flow cytometry: (a) control HeLa cells and IC_{50} concentrations of drug treatment (b) TiH_2L^2, (c) TiH_2L^3, (d) TiH_2L^4, (e) bar graph and (f) tabular depiction of the various phases of the cell cycle after varying treatments with the complexes (TiH_2L^2–TiH_2L^4).

results in cell death. Thus, anticancer drugs should be capable of increasing the intracellular ROS level to damage the cancer cells.

To evaluate and confirm the quantitative generation of ROS during the treatment by **TiH_2L^2–TiH_2L^4** with their respective IC_{50} concentrations, treated HeLa cells were compared with control wells by flow cytometry. As intracellular ROS production becomes elevated enough, it causes cell death as an indication of cellular stress.[55,74] The increased ROS levels reflect a higher fluorescence intensity. Fig. 11 displays the observed ROS percentage in control cells as 45.86%, whereas the percentage ROS generation of the cells was elevated after treatment with IC_{50} concentrations of **TiH_2L^2–TiH_2L^4**. Interestingly, the ROS generation of **TiH_2L^2**, **TiH_2L^3** and **TiH_2L^4** was found to be 68.42%, 77.99% and 68.64%, respectively. Complex **TiH_2L^3** exhibits the highest ROS generation, and complexes **TiH_2L^2** and **TiH_2L^4** display almost the same activity.

2.21 Apoptosis in A549 cells by annexin V-APC/PI assay

Naturally, the proteins and peptides that comprise cellular components that PCD (programmed cell death) have begun to be degraded/broken down by a class of caspase enzymes known as cystine proteases. There are two separate pathways to activate caspases, called the intrinsic pathway, which is mediated by mitochondria, and the extrinsic pathway, which is mediated by death receptors. The binding of a death receptor with drugs (metal complexes) is a causative agent for initiating an apoptosis cascade. The cell membrane is unbroken in the early phases of apoptosis, but eventually it breaks down and turns 'leaky.' As a result, flow cytometry could be used to determine the stages of cell death by measuring cell surface binding, by employing Annexin V in conjunction with a dye PI exclusion test, and it reflects whether the integrity of the cell membrane is lost. Hence, healthy cell populations could be identified from apoptotic (dying) or necrotic cell populations by their inability to bind Annexin V and their exclusion of PI.[19,26]

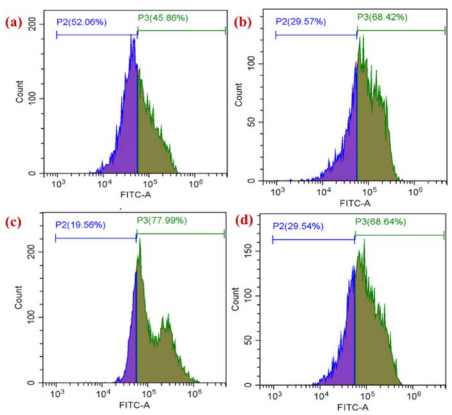

Fig. 11 Quantitative analysis of ROS production from HeLa cells treated with titanium(IV) complexes: (a) control cells, (b) TiH_2L^2, (c) TiH_2L^3 and (d) TiH_2L^4 by flow cytometric analysis.

The IC_{50} concentrations of each titanium(IV) derivative (**TiH_2L^2–TiH_2L^4**) were used to treat HeLa cells and were found to exhibit considerable apoptotic initiation, as observed using an Annexin V-APC/PI assay. The untreated HeLa cells exhibited 87.94% live cells, and there was no apoptotic phase, whereas **TiH_2L^2**-loaded HeLa cells displayed a significant apoptosis phase (viable cells: 68.87; early apoptosis: 22.84%; late apoptosis: 8.04% and necrosis: 0.25%) (Fig. 12). Viable cells were found, while **TiH_2L^3**-loaded HeLa cells displayed significant apoptosis (viable cells: 73.65; early apoptosis: 22.88%; late apoptosis: 3.28% and necrosis: 0.19%). Similarly, observations obtained from **TiH_2L^4**-loaded HeLa display a cell with a considerable necrotic phase and with increased viability of cells (viable cells: 76.37; early apoptosis: 19.58%; late apoptosis: 3.69% and necrosis: 0.38%). Thus, above-mentioned findings suggest the apoptosis-inducing potential of complexes **TiH_2L^2–TiH_2L^4** against HeLa cells.

Complex **TiH_2L^3** displayed 22.88% cell death in the lower IC_{50} concentration (14.7 μg), indicating that cell death evidently occurred in an apoptosis manner, even though complex **TiH_2L^3** showed a lower percentage of early apoptosis compared to previous studies. According to relevant reports, mitochondria

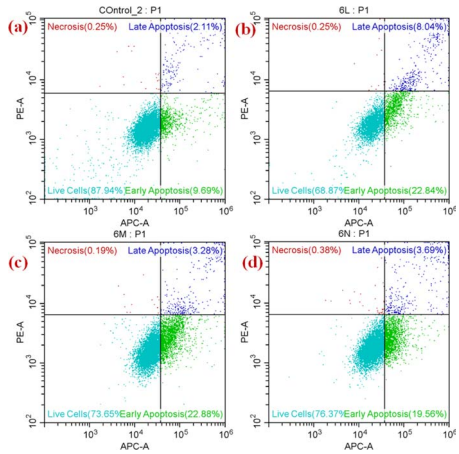

Fig. 12 Apoptosis assay by flow cytometry: (a) untreated cells of HeLa, and apoptosis of HeLa cells after treatment with IC_{50} concentrations of each complex: (b) TiH_2L^2, (c) TiH_2L^3 and (d) TiH_2L^4.

are essential for the initial phase of apoptosis because they release cytochrome C. In the present investigation, cell death may occur in cell cycle analysis through apoptosis, which might be releasing cytochrome C. In view of studies mentioned in the literature, the intrinsic apoptosis pathway causes a loss of intracellular water, which leads to the cytoplasm condensing and altering the size, shape and adhesion of the cell.[19,26,43]

3. Experimental section

3.1 Materials and methods

The new metallacyclic derivatives of titanium(IV) were synthesized under moisture-free conditions. Titanium(IV) isopropoxide and NMR solvents were purchased from Sigma Aldrich and tetrahydrofuran (THF), hexane and dichloromethane were procured from Purechem. Salicylaldehyde, aniline derivatives, sodium carbonate, sodium nitrite and ethanol were outsourced from Avra chemicals. Solvents such as THF, hexane and dichloromethane were made anhydrous by refluxing with sodium wire as per the standard method.[75] The newly developed titanium(IV) complexes were characterized by spectroscopic techniques such as NMR by recording data on a Bruker ADVANCE III (400 MHz frequencies for ^1H & ^{13}C) spectrophotometer using deuterated DMSO as solvent and tetramethyl silane (TMS) as an internal reference. Chemical shift values are assigned in parts per million (ppm). The DMSO-d_6 peak was observed at 2.5 ppm, and its moisture absorption peak was visible at 3.33 ppm. The melting point and FTIR spectra were recorded on an Elchem digital melting point apparatus and Shimadzu IR Affinity 1 (4000–400) spectrometer using anhydrous KBr pellets, respectively. UV-visible spectra were recorded on a Jasco V-670 UV-visible spectrophotometer, and HRMS spectra were observed on a Waters-Xevo G2-XS-Q TOF.

3.2 Synthesis of azo-based tridentate ONO-type ligands

The (*E*)-2-hydroxy-4-(phenyldiazenyl)benzaldehyde derivatives (H_1L^1–H_1L^5) and tridentate ligands 2-((*E*)-((2-hydroxyphenyl)imino)methyl)-5-((*E*)-phenyldiazenyl)phenol (H_2L^1–H_2L^5) of the current series of work were prepared and purified by reported methods,[60] and their structures were verified by relevant spectral techniques. The ligand derivatives (H_2L^1–H_2L^5) were prepared by treating 20 mL of ethanolic solution of (*E*)-2-hydroxy-4-(phenyldiazenyl)benzaldehyde derivatives with 2-amino phenol in a 1 : 1 molar ratio. Subsequently, the reaction mixture was refluxed at 90 °C for 6 h. During the course of refluxing, a reddish brown solid appeared and completion of the reaction was ensured by thin layer chromatography (TLC), and it was continued until the accomplishment of the reaction. Then once the reaction mixture had been obtained at normal temperature, the crude reddish solid product was filtered and recrystallized with THF/EtOH to obtain a reddish brown powder as pure ligands (H_2L^1–H_2L^5) and dried in a hot-air oven for 48 h. Structural elucidation of H_2L^1–H_2L^5 was executed with NMR (^1H and ^{13}C) and FTIR spectroscopic techniques.

3.3 Synthesis of new titanium(IV) derivatives (TiH_2L^1–TiH_2L^5)

Titanium(IV) compounds (**TiH_2L^1–TiH_2L^5**) were successfully synthesised by refluxing tridentate ligand derivatives 2-((*E*)-((2-hydroxyphenyl)imino)methyl)-5-((*E*)-phenyldiazenyl)phenol (H_2L^1–H_2L^5) with titanium tetraisopropoxide in 2 : 1 stoichiometry in dry THF over 24 h (Scheme 1). The synthetic methodology adopted for compound **TiH_2L^1** could also be generalized to develop the other complexes (**TiH_2L^2–TiH_2L^5**) of the series.

3.4 Synthesis of TiH_2L^1 [$(C_{38}H_{26}N_6O_4)Ti$]

An anhydrous THF solution (*ca.* 10 mL) of 2-((*E*)-((2-hydroxyphenyl)imino)methyl)-5-((*E*)-phenyldiazenyl)phenol (1.07 g, 34 mmol) was added to 10 mL of dry THF solution containing titanium(IV) isopropoxide (0.5 g, 17 mmol) in 2 : 1 stoichiometry. The reaction mixture immediately turned reddish brown and was refluxed using a perfectly dried fractionating column at 90 °C for 24 h. After completion of the reaction, excess THF was removed under reduced pressure to obtain a reddish solid. The crude solid was further washed with ethyl acetate and *n*-hexane (3 : 7) thrice to get a reddish brown solid of complex **TiH_2L^1**. Yield: 0.75 g (89%). M. p. > 320 °C. ^1H NMR (400 MHz, DMSO-d_6) δ (ppm): 9.71 (s, 2H), 8.94 (s, 2H), 8.54–8.54 (d, 2H, $J = 1.2$ Hz), 7.91–7.89 (d, 5H, $J = 3.6$ Hz), 7.81–7.78 (d, 6H, $J = 4.4$ Hz), 7.36 (s, 5H), 6.90–6.89 (d, 2H, $J = 1.6$ Hz), and 6.44–6.42 (d, 2H, $J = 4$ Hz). ^{13}C NMR (100 MHz, DMSO-d_6) δ (ppm): 164.06, 151.25, 150.94, 130.15, 129.93, 124.55, 124.42, 123.210, 119.84, 119.13, 118.89, 116.62, 114.11, 111.25. FTIR (solid KBr, ν in cm^{-1}): 2997, 1603, 1530, 1452, 1362, 1292, 1258, 1107, 1027, 830, 732, 624, 535, and 493. HRMS: calcd $[M^+]$ m/z 678.1495; found $[M + H]^+$ 679.1853.

3.5 Synthesis of TiH_2L^2 [$(C_{38}H_{24}F_2N_6O_4)Ti$]

An anhydrous THF solution of 5-((*E*)-(4-fluorophenyl)diazenyl)-2-((*E*)-((2-hydroxyphenyl)imino)methyl)phenol (1.20 g, 34 mmol) and $Ti(OPr^i)_4$ (0.5 g, and 17 mmol) afforded a reddish brown powder as complex **TiH_2L^2**. Yield: 0.75 g (85%). M. p. >

320 °C. ^{1}H NMR (400 MHz, DMSO-d_6) δ (ppm): 9.70 (s, 2H), 8.53 (s, 2 Hz), 7.98–7.95 (m, 4H), 7.80–7.78 (d, 2H, J = 4 Hz), 7.47–7.43 (t, 4H, J = 8.6 Hz), 7.14–7.10 (t, 2H, J = 7.6 Hz), 6.92–6.87 (q, 4H, J = 6.9 Hz), and 6.43–6.41 (d, 2H, J = 4 Hz). ^{13}C NMR (100 MHz, DMSO-d_6) δ (ppm): 163.82, 151.24, 145.15, 130.01, 129.92, 125.05, 124.96, 124.53, 124.34, 123.03, 119.84, 119.12, 118.81, 117.01, 116.81, 116.61, 116.58, 114.14, 111.28. FTIR (solid KBr, ν in cm^{-1}): 2998, 1602, 1532, 1467, 1371, 1294, 1229, 1110, 1030, 836, 735, 624, 537, and 479. HRMS: calcd [M$^+$] m/z 714.1307; found [M + H]$^+$ 715.3406.

3.6 Synthesis of TiH_2L^3 [($C_{38}H_{24}Cl_2N_6O_4$)Ti]

An anhydrous THF solution of 5-((*E*)-(4-chlorophenyl)diazenyl)-2-((*E*)-((2-hydroxyphenyl)imino)methyl)phenol (1.19 g, 34 mmol) was treated with titanium tetraisopropoxide (0.5 g, 17 mmol) to result in reddish brown solid of complex **TiH_2L^3**. Yield: 0.75 g (90%). M. p. > 320 °C. ^{1}H NMR (400 MHz, DMSO-d_6) δ (ppm): 9.70 (s, 2H), 8.54 (s, 2H), 8.13–8.08 (t, 3H, J = 6.4 Hz), 7.92–7.90 (d, 4H, J = 4.2 Hz), 7.80–7.78 (d, 2H, J = 4 Hz), 7.69–7.67 (d, 3H, J = 4.2 Hz), 7.14–7.11 (t, 2H, J = 3.8 Hz), 6.92–6.87 (q, 4H, J = 6.8 Hz), and 6.43–6.41 (d, 3.8 Hz). ^{13}C NMR (100 MHz, DMSO-d_6) δ (ppm): 164.01, 151.22, 150.92, 145.19, 136.00, 129.97, 129.86, 129.79, 124.76, 124.48, 124.31, 122.97, 119.79, 119.73, 119.07, 118.77, 116.87, 116.58, 114.01, and 111.15. FTIR (solid KBr, ν in cm^{-1}): 2982, 1601, 1530, 1458, 1366, 1291, 1256, 1113, 1083, 832, 737, 635, 544, and 445. HRMS: calcd [M$^+$] m/z 746.0716; found [M + H]$^+$ 747.1385.

3.7 Synthesis of TiH_2L^4 [($C_{38}H_{24}Br_2N_6O_4$)Ti]

A moisture-free THF solution of 5-((*E*)-(4-bromophenyl)diazenyl)-2-((*E*)-((2-hydroxyphenyl)imino)methyl)phenol (1.34 g, 34 mmol) was treated with Ti(OPr^i)$_4$ (0.5 g, 17 mmol) and produced a reddish brown solid **TiH_2L^4**. Yield: 0.75 g (90%). M. p. > 320 °C. ^{1}H NMR (400 MHz, DMSO-d_6) δ (ppm): 9.69 (s, 2H), 8.54 (s, 2H), 8.10–8.07 (d, 2H, J = 5.4 Hz), 7.85–7.77 (q, 10H, J = 8.8 Hz), 7.14–7.10 (t, 2H, J = 7.6 Hz), 6.92–6.87 (q, 4H, J = 7 Hz), and 6.43–6.41 (d, 2H, J = 4 Hz). ^{13}C NMR (100 MHz, DMSO-d_6) δ (ppm): 164.06, 151.23, 145.18, 132.81, 130.04, 129.90, 124.77, 124.67, 124.59, 124.52, 123.04, 119.83, 119.75, 119.09, 118.83, 116.89, 116.60, 114.03, and 111.16. FTIR (solid KBr, ν in cm^{-1}): 2992, 1602, 1524, 1470, 1363, 1294, 1250, 1148, 1018, 832, 743, 624, 546, and 457. HRMS: calcd [M$^+$] m/z 833.9705; found [M + H]$^+$ 834.9783.

3.8 Synthesis of TiH_2L^5 [($C_{38}H_{24}N_8O_8$)Ti]

THF solution of 2-((*E*)-((2-hydroxyphenyl)imino)methyl)-5-((*E*)-(4-nitrophenyl)diazenyl)phenol (1.23 g, 34 mmol) was refluxed with Ti(OPr^i)$_4$ (0.5 g, 17 mmol) to obtain complex **TiH_2L^5** as a reddish brown solid. Yield: 0.75 g (88%). M. p. > 320 °C. ^{1}H NMR (400 MHz, DMSO-d_6) δ (ppm): 10.42 (s, 2H), 8.26–8.26 (d, 2H, J = 2.4 Hz), 8.15–8.12 (q, 2H, J = 4.8 Hz), 7.86–7.79 (q, 8H, J = 8.6 Hz), 7.34–7.24 (m, 6H), 7.08–7.06 (d, 2H, J = 8 Hz), and 6.94–6.91 (t, 2H, J = 7.6 Hz). ^{13}C NMR (100 MHz, DMSO-d_6) δ (ppm): 164.05, 151.23, 145.19, 132.81, 130.04, 129.90, 124.77, 124.67, 124.59, 124.52, 123.04, 119.83, 119.75, 119.09, 118.83, 116.89, 116.60, 114.02, and 111.16. FTIR (solid KBr, ν in cm^{-1}): 2998, 1603, 1520, 1458, 1337, 1293, 1251, 1103, 1022, 843, 736, 622, 533, and 434. HRMS: calcd [M$^+$] m/z 768.1197; found [M + H]$^+$ 769.1271.

3.9 UV-visible and fluorescence studies

To investigate the photo-physical properties of titanium(IV) complexes (**TiH_2L^1–TiH_2L^5**), were evaluated by UV-visible and fluorescence spectroscopic techniques.[61,66] The comparative William's approach, which includes a well-characterized reference with a known quantum yield value, and an aqueous solution of 10% DMSO (dimethyl sulfoxide) was used to compute the fluorescence quantum yield (φ). Quinine sulphate was employed as a reference sample (0.54 in 0.1 M H_2SO_4), where excitation was spotted at 350 nm, while emission was located at 450 nm. The quantum yield could be determined as in eqn (1):

$$\varphi = \varphi_R \times \frac{I_S}{I_R} \times \frac{OD_R}{OD_S} \times \eta_S/\eta_R, \quad (1)$$

where φ = quantum yield, OD = absorbance at λ_{max}, I = peak area, η = refractive index of solvent (S) and reference (R).

3.10 Density functional theory

State-of-the-art methods were performed using Gaussian 09 (G 09) computational codes by applying Becke's three-parameter hybrid exchange and Lee–Yang–Parr non-local correlation functionals (B3LYP) using density functional theory (DFT). For all calculations, the standard basis set was 6-311G(d,p) for lighter elements, and LanL2DZ was the effective core potential for the metal. The geometry of **TiH_2L^1–TiH_2L^5** was optimized to zero negative vibration frequency to represent the local minima associated with positive eigenvalues only. Vertical electronic excitations based on B3LYP were obtained with time-dependent density functional theory (TD-DFT) using the ground-state optimized geometry.[76] To account for the solvent effect, DFT and TD-DFT were associated with the conductor-like polarizable continuum model (CPCM) in water.[77]

3.11 CT-DNA binding studies

To assess the binding interaction of the titanium(IV) derivatives (**TiH_2L^1–TiH_2L^5**) with DNA, UV-visible absorption titration was carried out using 5 mM phosphate-buffered saline (PBS, pH-7.2). The initial concentration of DNA was calculated from the absorbance intensity of DNA detected at 260 nm and was named the molar absorption coefficient value (6600 M^{-1} cm^{-1}).[61,65] Stock solutions of **TiH_2L^1–TiH_2L^5** were prepared in DMSO, and dilutions of these derivatives were performed with PBS buffer. The titration experiments were carried out with increasing concentrations of CT-DNA (0–50 μM) into a constant concentration of **TiH_2L^1–TiH_2L^5**. Eqn (2) could be used to determine the intrinsic DNA binding constant (K_b):

$$\frac{[DNA]}{(\varepsilon_a - \varepsilon_f)} = \frac{[DNA]}{(\varepsilon_a - \varepsilon_f)} + \frac{1}{kb(\varepsilon_a - \varepsilon_f)}, \quad (2)$$

where [DNA] denotes the quantity of DNA contained within the base pairs, ε_a corresponds to the apparent extinction coefficient of the complexes, the extinction coefficient of complexes in

their free form is represented by ε_f and becomes ε_b when derivatives are fully bonded with DNA. The UV-visible absorption data were plotted with [DNA]/($\varepsilon_a - \varepsilon_f$) *vs.* [DNA].

3.12 EtBr displacement assay

Furthermore, the competitive binding of complexes **TiH_2L^1–TiH_2L^5** with ethidium bromide (EtBr, fluorophore) bound DNA was investigated by fluorometry. Stock solutions of EtBr (8 μM) and DNA (120 μM) were separately prepared in PBS buffer, but their rational mixture was used as reference solution and that displayed excitation at 480 nm, while emission was at 596 nm. Eqn (3) was used to determine the values of the apparent binding constant (K_{app}):

$$k_{app} \times [complex]_{50} = k_{EtBr} \times [EtBr], \quad (3)$$

where k_{EtBr}, denotes the EtBr binding constant ($k_{EtBr} = 1.0 \times 10^7$ M^{-1}) and [EtBr] = 8×10^{-6} M. The quantifiable quenching constant (K_{SV}) was determined from the Stern–Volmer eqn (4). Fluorescence data of the binding interaction was used to find the linear plot of I_0/I *vs.* [complex].[61]

$$I_0/I = 1 + K_{SV}[Q], \quad (4)$$

where I_0 and I denote the fluorescence intensities in the absence and in presence of the complexes, respectively.

3.13 ^{1}H NMR spectroscopy

^{1}H NMR data were recorded on a Bruker ADVANCE III (400 MHz frequencies for ^{1}H & ^{13}C) spectrophotometer at 298 K using deuterated DMSO-d_6 + D_2O (2 : 3) as the solvent and tetramethyl silane (TMS) as an internal reference. Complex **TiH_2L^3** (5 mg) was dissolved in a mixture of DMSO-d_6 + D_2O solvents, and for comparison, the system CT-DNA-**TiH_2L^3** was prepared using 5 mg of CT-DNA and 5 mg of **TiH_2L^3** together. In all ^{1}H NMR experiments; 0.5 mL of sample solution was added into clean NMR tubes. Afterwards, data obtained from the NMR spectra were processed with Bruker TopSpin 4.0.5 software.[26,67]

3.14 BSA interactions

Significant functions in drug transport and metabolism are regulated by serum albumin proteins that form a prominent portion of blood plasma proteins, and BSA is also a structural homologue of human serum albumin (HSA). An initial standard solution of BSA (5 μM) was prepared using PBS buffer and stored at 2–6 °C before the experiment. The binding interactions of BSA with newly developed titanium(IV) complexes (**TiH_2L^1–TiH_2L^5**) were studied by UV-visible absorption titration in the range of 200 to 800 nm, and tryptophan emission quenching studies were also performed. Changes observed in the absorption and fluorescence intensity at a constant excitation of 280 nm and emission of 344 nm could be attributed to quenching interactions of BSA with individual metal complexes. The intensity of BSA at λ_{max} (344 nm) was found to be gradually decreased by the addition of diverse concentrations (0–20 μM) of titanium(IV) complexes, which confirms the interaction between the derivatives **TiH_2L^1–TiH_2L^5** and BSA. The Stern–Volmer eqn (5) was used to quantitatively calculate the quenching constant, and the spectral data of emission were used to obtain the linear plot of I_0/I *vs.* [complex].

$$I_0/I = 1 + K_{BSA}[Q] = 1 + K_q\tau_0[Q], \quad (5)$$

where I_0 and I denote the fluorescence intensities of BSA in the absence and presence of complex [Q], respectively, τ_0 denotes the lifetime of tryptophan in BSA, and K_q represents the quenching constant. The Scatchard eqn (6) gives the determination of binding sites (n) and binding constant (k) properties of the complexes,

$$\log(I_0 - I)/I = \log k + n \log[Q] \quad (6)$$

3.15 Circular dichroism (CD)

CD spectra were obtained to map possible conformational alterations for CT-DNA (120 μM) and BSA (5 μM) that occurred in the presence of **TiH_2L^2–TiH_2L^4** (20 μM for BSA and 50 μM for CT-DNA) by detecting them on a JASCO J-815 CD spectropolarimeter using a quartz cuvette of path length 0.1 cm at 1 nm data pitch intervals.[67] The CD spectra were recorded between 200 and 300 nm wavelength, and throughout the experiment, the spectropolarimeter was continuously fluxed with nitrogen to absorb moisture, and PBS (pH-7.2) was used as a blank control. Each experiment was carried out in triplicate to suppress the noise ratio of the signals.

3.16 Molecular docking

A docking experiment was carried out to find the most stable binding configuration with the maximum interaction mode, binding energy and affinity of the corresponding derivatives for DNA and BSA. The synthesized complexes **TiH_2L^1–TiH_2L^5** were exposed to a molecular docking study using Autodock 4.2, covering the Lamarckian Genetic Algorithm (LGA) to calculate the binding affinities of several conformers and AutoDock Tools (ADT) to implement the operation and subsequent calculations. The crystallographic structure of DNA with the sequence d(CpGpCpGpApApTpTpCpGpCpG) (PDB ID: 1BNA) and crystallographic structure of BSA (PDB ID: 4F5S) retrieved from the protein data bank (**https://www.rcsb.org/pdb**)[78,79] with a resolution of 1.90 Å was built using the Autodock 4.2 package to establish the BSA and DNA-binding properties of **TiH_2L^1–TiH_2L^5**. These Ti(IV) complexes were molecularly docked with crystal structured BSA protein (PDB ID: 4F5S) and DNA (PDB ID: 1BNA) and examined. To prevent undesirable contact with docked conformers, water molecules were additionally omitted throughout the protein preparation process. The optimized 3D structures of the complexes **TiH_2L^1–TiH_2L^5** derived from DFT were converted into PDB format through Gaussian 09 (G 09) computational codes. For all the calculations, the standard basis set 6-311G (d,p) was used for lighter elements and LanL2DZ effective core potential for the metal. Before docking, the binding site was assigned in developing a grid box with

a spacing of 0.7 Å and 40 × 40 × 40 points in *x*, *y* and *z* directions. In the case of BSA, the grid size was considered to be 40 × 40 × 40 points in *x*, y and *z* with a spacing of 1 Å encircling all the putative active site residues of BSA (Trp213 and Trp134). The working principle and the output parameters were similar to the above-mentioned DNA docking. Interpretation of the docked pose was carried out *via* LIGPLOT and PyMol molecular visuals programs.

4. Conclusions

The present investigation deals with the synthesis of five new homoleptic homonuclear titanium(IV) derivatives (**TiH_2L^1**–**TiH_2L^5**) and their characterization with relevant spectroscopic techniques. CT-DNA binding interaction with **TiH_2L^1**–**TiH_2L^5** demonstrated their favourable DNA intercalative tendency, while a strong affinity for BSA static quenching reflected simple bloodstream transport into the cellular medium. Newly developed scaffolds demonstrated quite noteworthy anti-proliferative activities against HeLa and A549 cell lines. Further, it was observed that the complex **TiH_2L^3** sparklingly achieved dominance over analogous because of its outstanding potency in conjugation and greater binding sites for CT-DNA, BSA and cancer cells. Thus, observed data and their description could enable these findings to be enlisted in the fraternity of anti-cancer theranostic drugs.

Author contributions

Sathish Thanigachalam: scheme development; experimental section; data collection and consolidation; manuscript preparation. Madhvesh Pathak: conceptualization; supervision; data analysis and interpretation; manuscript correction; resources; administrative and infrastructure facilities; expert advices on investigation.

Conflicts of interest

In considered opinion, authors announce that 'there is no conflict of interest at all' in the publication of this manuscript'.

Acknowledgements

'VIT Seed Grant (SG20230068)' of the Vellore Institute of Technology Vellore, Tamil Nadu, India is acknowledged sincerely to support the present research work. Authors extend their thankfulness to Dr Gothandam K. M., Professor, SBST, VIT Vellore for carrying out cytotoxicity of the titanium(IV) complexes.

References

1 D. X. West, A. E. Liberta, S. B. Padhye, R. C. Chikate, P. B. Sonawane, A. S. Kumbhar and R. G. Yerande, Thiosemicarbazone complexes of copper (II): structural and biological studies, *Coord. Chem. Rev.*, 1993, **123**, 49–71.
2 J. Reedijk, Why does cisplatin reach guanine-N7 with competing S-donor ligands available in the cell?, *Chem. Rev.*, 1999, **99**, 2499–2510.
3 V. Cepeda, M. A. Fuertes, J. Castilla, C. Alonso, C. Quevedo and J. M. Pérez, Biochemical mechanisms of cisplatin cytotoxicity, *Anti-Cancer Agents Med. Chem.*, 2007, **7**, 3–18.
4 N. Ganot, O. Briaitbard, A. Gammal, J. Tam, J. Hochman and E. Y. Tshuva, In vivo anti-cancer activity of a nontoxic inert phenolato titanium complex: high efficacy on solid tumors alone and combined with platinum drugs, *ChemMedChem*, 2018, **13**, 2290–2296.
5 H. Köpf and P. Köpf-Maier, Titanocene dichloride—the first metallocene with cancerostatic activity, *Angew. Chem., Int. Ed. Engl.*, 1979, **18**, 477–478.
6 H. Köpf, S. Grabowski and R. Voigtländer, Spektrometrische und präparative untersuchungen zur hydrolyse von titanocendichlorid, *J. Organomet. Chem.*, 1981, **216**, 185–190.
7 E. Meléndez, Titanium complexes in cancer treatment, *Crit. Rev. Oncol. Hematol.*, 2002, **42**, 309–315.
8 P. M. Abeysinghe and M. M. Harding, Antitumour bis (cyclopentadienyl) metal complexes: titanocene and molybdocene dichloride and derivatives, *Dalton Trans.*, 2007, **32**, 3474–3482.
9 P. Köpf-Maier and H. Köpf, Transition and main-group metal cyclopentadienyl complexes: preclinical studies on a series of antitumor agents of different structural type, *InBioinorganic Chemistry*, Springer Berlin Heidelberg, Berlin, Heidelberg, 2005, pp. 103–185.
10 G. Kelter, N. J. Sweeney, K. Strohfeldt, H. H. Fiebig and M. Tacke, In vitro anti-tumor activity studies of bridged and unbridged benzyl-substituted titanocenes, *Drugs*, 2005, **16**, 1091–1098.
11 K. Strohfeldt and M. Tacke, Bioorganometallic fulvene-derived titanocene drugs, *Chem. Soc. Rev.*, 2008, **37**, 1174–1187.
12 M. Cini, T. D. Bradshaw and S. Woodward, Using titanium complexes to defeat cancer: the view from the shoulders of titans, *Chem. Soc. Rev.*, 2017, **46**, 1040–1051.
13 K. M. Buettner and A. M. Valentine, Bioinorganic chemistry of titanium, *Chem. Rev.*, 2012, **112**, 1863–1881.
14 T. Zhao, P. Wang, N. Liu, S. Li, M. Yang and Z. Yang, Facile synthesis of [ONON] type titanium (IV) bis-chelated complexes in alcoholic solvents and evaluation of anti-tumor activity, *J. Inorg. Biochem.*, 2022, **235**, 111925.
15 M. Scarpi-Luttenauer, K. Galentino, C. Orvain, M. Cecchini, C. Gaiddon and P. Mobian, TiO4N2 complexes formed with 1, 10-phenanthroline ligands containing a donor-acceptor hydrogen bond site: Synthesis, cytotoxicity and docking experiments, *Inorg. Chim. Acta*, 2022, **540**, 121036.
16 M. Miller, A. Mellul, M. Braun, D. Sherill-Rofe, E. Cohen, Z. Shpilt, I. Unterman, O. Braitbard, J. Hochman, E. Y. Tshuva and Y. Tabach, Titanium tackles the endoplasmic reticulum: a first genomic study on a titanium anti-cancer metallodrug, *iScience*, 2020, **23**, 101262.
17 J. H. Bannon, I. Fichtner, A. O'Neill, C. Pampillón, N. J. Sweeney, K. Strohfeldt, R. W. Watson, M. Tacke and

M. M. Mc Gee, Substituted titanocenes induce caspase-dependent apoptosis in human epidermoid carcinoma cells in vitro and exhibit antitumour activity in vivo, *Br. J. Cancer*, 2007, **97**, 1234–1241.

18 C. Pampillón, J. Claffey, M. Hogan and M. Tacke, Novel achiral titanocene drugs synthesised from bis-N, N-dimethylamino fulvene and lithiated heterocyclic compounds, *BioMetals*, 2008, **21**, 197–204.

19 M. Cini, T. D. Bradshaw and S. Woodward, Using titanium complexes to defeat cancer: the view from the shoulders of titans, *Chem. Rev.*, 2017, **46**, 1040–1051.

20 Z. Shpilt and E. Y. Tshuva, Binding of the anticancer Ti (IV) complex phenolaTi to serum proteins: Thermodynamic and kinetic aspects, *J. Inorg. Biochem.*, 2022, **232**, 111817.

21 A. M. Pizarro, A. Habtemariam and P. J. Sadler, Activation mechanisms for organometallic anticancer complexes, *Medicinal Organometallic Chemistry*, 2010, pp. 21–56.

22 M. Guo, H. Sun, H. J. McArdle, L. Gambling and P. J. Sadler, TiIV uptake and release by human serum transferrin and recognition of TiIV-transferrin by cancer cells: understanding the mechanism of action of the anticancer drug titanocene dichloride, *Biochem*, 2000, **39**, 10023–10033.

23 A. D. Tinoco and A. M. Valentine, Ti (IV) binds to human serum transferrin more tightly than does Fe(III), *J. Am. Chem. Soc.*, 2005, **127**, 11218–11219.

24 A. D. Tinoco, C. D. Incarvito and A. M. Valentine, Calorimetric, spectroscopic, and model studies provide insight into the transport of Ti (IV) by human serum transferrin, *J. Am. Chem. Soc.*, 2007, **129**, 3444–3454.

25 C. P. Tan, Y. Y. Lu, L. N. Ji and Z. W. Mao, Metallomics insights into the programmed cell death induced by metal-based anticancer compounds, *Metallomics*, 2014, **6**, 978–995.

26 S. U. Rehman, T. Sarwar, M. A. Husain, H. M. Ishqi and M. Tabish, Studying non-covalent drug–DNA interactions, *Arch. Biochem. Biophys.*, 2015, **576**, 49–60.

27 T. A. Immel, M. Grützke, E. Batroff, U. Groth and T. Huhn, Cytotoxic dinuclear titanium-salan complexes: Structural and biological characterization, *J. Inorg. Biochem.*, 2012, **16**, 68–75.

28 F. Caruso, L. Massa, A. Gindulyte, C. Pettinari, F. Marchetti, R. Pettinari, M. Ricciutelli, J. Costamagna, J. C. Canales, J. Tanski and M. Rossi, (4-Acyl-5-pyrazolonato) titanium Derivatives: Oligomerization, Hydrolysis, Voltammetry, and DFT Study, *Eur. J. Inorg. Chem.*, 2003, **17**, 3221–3232.

29 G. Nahari and E. Y. Tshuva, Synthesis of asymmetrical diaminobis (alkoxo)-bisphenol compounds and their C 1-symmetrical mono-ligated titanium (iv) complexes as highly stable highly active antitumor compounds, *Dalton Trans.*, 2021, **50**, 6423–6426.

30 I. Kostova, Titanium and vanadium complexes as anti-cancer agents, *Anti-Cancer Agents Med. Chem.*, 2009, **9**, 827–842.

31 M. Miller, A. Mellul, M. Braun, D. Sherill-Rofe, E. Cohen, Z. Shpilt, I. Unterman, O. Braitbard, J. Hochman, E. Y. Tshuva and Y. Tabach, Titanium tackles the endoplasmic reticulum: a first genomic study on a titanium anticancer metallodrug, *iScience*, 2020, **23**, 101262.

32 T. A. Immel, M. Grützke, A. K. Späte, U. Groth, P. Öhlschläger and T. Huhn, Synthesis and X-ray structure analysis of a heptacoordinate titanium (IV)-bis-chelate with enhanced in vivo antitumor efficacy, *Chem. Commun.*, 2012, **48**, 5790–5792.

33 M. Grützke, T. Zhao, T. A. Immel and T. Huhn, Heptacoordinate heteroleptic salan (ONNO) and thiosalan (OSSO) titanium (IV) complexes: investigation of stability and cytotoxicity, *Inorg. Chem.*, 2015, **54**, 6697–6706.

34 Z. Shpilt, R. Manne, M. A. Rohman, S. Mitra, E. R. Tiekink, T. S. Basu Baul and E. Y. Tshuva, Homoleptic Ti [ONO] 2 type complexes of amino-acid-tethered phenolato Schiff-base ligands: Synthesis, characterization, time-resolved fluorescence spectroscopy, and cytotoxicity against ovarian and colon cancer cells, *Appl. Organomet. Chem.*, 2020, **34**, e5309.

35 E. Y. Tshuva and D. Peri, Modern cytotoxic titanium (IV) complexes; Insights on the enigmatic involvement of hydrolysis, *Coord. Chem. Rev.*, 2009, **253**, 2098–2115.

36 S. Meker, K. Margulis-Goshen, E. Weiss, S. Magdassi and E. Y. Tshuva, High antitumor activity of highly resistant salan-titanium (IV) complexes in nanoparticles: an identified active species, *Angew. Chem., Int. Ed. Engl.*, 2012, **51**, 10515–10517.

37 C. M. Manna, O. Braitbard, E. Weiss, J. Hochman and E. Y. Tshuva, Cytotoxic Salan–Titanium (IV) Complexes: High Activity Toward a Range of Sensitive and Drug-Resistant Cell Lines, and Mechanistic Insights, *ChemMedChem*, 2012, **7**, 703–708.

38 M. Shavit, D. Peri, C. M. Manna, J. S. Alexander and E. Y. Tshuva, Active cytotoxic reagents based on non-metallocene non-diketonato well-defined C 2-symmetrical titanium complexes of tetradentate bis (phenolato) ligands, *J. Am. Chem. Soc.*, 2007, **129**, 12098–12099.

39 H. Glasner and E. Y. Tshuva, C 1-symmetrical titanium (IV) complexes of salan ligands with differently substituted aromatic rings: Enhanced cytotoxic activity, *Inorg. Chem.*, 2014, **53**, 3170–3176.

40 S. Barroso, A. M. Coelho, S. Gómez-Ruiz, M. J. Calhorda, Ž. Žižak, G. N. Kaluđerović and A. M. Martins, Synthesis, cytotoxic and hydrolytic studies of titanium complexes anchored by a tripodal diamine bis (phenolate) ligand, *Dalton Trans.*, 2014, **43**, 17422–17433.

41 M. Taha and E. Y. Tshuva, Phenolato Ti (iv) hexacoordinate complexes for anticancer chemotherapy: enhancement of solubility, hydrolytic stability, and cytotoxicity, *Dalton Trans.*, 2023, **52**, 7664–7672.

42 A. Pedko, E. Rubanovich, E. Y. Tshuva and A. Shurki, Hydrolytically Stable and Cytotoxic [ONO N] 2Ti (IV)-Type Octahedral Complexes, *Inorg. Chem.*, 2022, **61**, 17653–17661.

43 N. Kumar, R. Kaushal, A. Chaudhary, S. Arora and P. Awasthi, Titanium based mixed ligand complexes: Synthesis, spectroscopic and in vitro antiproliferative studies, *Inorg. Nano-Met. Chem.*, 2018, **48**, 467–476.

44 (*a*) Y. Duo, G. Luo, Z. Li, Z. Chen, X. Li, Z. Jiang, B. Yu, H. Huang, Z. Sun and X. F. Yu, Photothermal and enhanced photocatalytic therapies conduce to synergistic anticancer phototherapy with biodegradable titanium diselenide nanosheets, *Small*, 2021, **17**, 2103239; (*b*) E. J. Park, S. Y. Lee, G. H. Lee, D. W. Kim, Y. Kim, M. H. Cho and J. H. Kim, Sheet-type titania, but not P25, induced paraptosis accompanying apoptosis in murine alveolar macrophage cells, *Toxicol. Lett.*, 2014, **230**, 69–79.

45 (*a*) U. Ndagi, N. Mhlongo and M. E. Soliman, Metal complexes in cancer therapy–an update from drug design perspective, *Drug Des., Dev. Ther.*, 2017, 599–616; (*b*) A. A. Sulaiman, H. M. Sobeai, E. Aldawood, A. Abogosh, K. Alhazzani, M. R. Alotaibi, S. Ahmad, A. Alhoshani and A. A. Isab, In vitro and in vivo antitumor studies of potential anticancer agents of platinum (II) complexes of dicyclopentadiene and dithiocarbamates, *Metallomics*, 2022, **14**, mfac054; (*c*) A. S. Arojojoye, J. H. Kim, C. Olelewe, S. Parkin and S. G. Awuah, Chiral gold (III) complexes: speciation, in vitro, and in vivo anticancer profile, *Chem. Commun.*, 2022, **58**, 10237–10240; (*d*) H. Q. Zhang, X. Lu, H. Liang and Z. F. Chen, Copper (II) complexes with plumbagin and bipyridines target mitochondria for enhanced chemodynamic cancer therapy, *J. Inorg. Biochem.*, 2024, **251**, 112432; (*e*) J. Haribabu, R. Arulkumar, D. Mahendiran, K. Jeyalakshmi, S. Swaminathan, P. Venuvanalingam, N. Bhuvanesh, J. F. Santibanez and R. Karvembu, Effect of coordination mode of thiosemicarbazone on the biological activities of its Ru (II)-benzene complexes: Biomolecular interactions and anticancer activity via ROS-mediated mitochondrial apoptosis, *Inorg. Chim. Acta*, 2024, 121973; (*f*) M. A. Ragheb, M. H. Soliman, I. A. Abdelhamid, M. M. Shoukry, M. Haukka and M. S. Ragab, Anticancer behaviour of 2, 2′-(pyridin-2-ylmethylene) bis (5, 5-dimethylcyclohexane-1, 3-dione)-based palladium (II) complex and its DNA, BSA binding propensity and DFT study, *J. Inorg. Biochem.*, 2024, **253**, 112488.

46 S. De, S. K. Subran, S. K. Ramasamy, S. Banerjee, P. Paira and A. K. Kalleshappa, Luminescent Anti-cancer Acenaphtho [1, 2-b] quinoxaline: Green Synthesis, DFT and Molecular Docking Studies, Live-Cell Imaging and Reactivity towards Nucleic Acid and Protein BSA, *ChemistrySelect*, 2018, **3**, 5421–5430.

47 R. Cole, Live-cell imaging: The cell's perspective, *Cell Adhes. Migr.*, 2014, **8**, 452–459.

48 A. D. Tinoco, E. V. Eames, C. D. Incarvito and A. M. Valentine, Hydrolytic metal with a hydrophobic periphery: titanium (IV) complexes of naphthalene-2, 3-diolate and interactions with serum albumin, *Inorg. Chem.*, 2008, **47**, 8380–8390.

49 D. Krishnan and A. Sheela, Design of Azomethine based Metalloorganic Complexes and their Binding Interactions with Nucleic Acid and Protein, *J. Mol. Struct.*, 2023, 137407.

50 B. Chakraborty and S. Basu, Interaction of BSA with proflavin: A spectroscopic approach, *J. Lumin.*, 2009, **129**, 34–39.

51 M. N. Uddin, M. S. Amin, M. S. Rahman, S. Khandaker, W. Shumi, M. A. Rahman and S. M. Rahman, Titanium (IV) complexes of some tetra-dentate symmetrical bis-Schiff bases of 1, 6-hexanediamine: Synthesis, characterization, and in silico prediction of potential inhibitor against coronavirus (SARS-CoV-2), *Appl. Organomet. Chem.*, 2021, **35**, e6067.

52 S. Thanigachalam and M. Pathak, Development of nano titania/polyvinylidene fluoride composite from new titanium (IV) derivative and its investigation on antibacterial, BSA interaction and cytotoxicity, *Mater. Today Commun.*, 2023, **35**, 105774.

53 B. Samuel, K. R. Ethiraj and M. Pathak, Moisture stable heteroleptic titanium (IV) complexes derived from 8-hydroxyquinoline: synthesis, antibacterial, and antifungal studies, *Med. Chem. Res.*, 2015, **24**, 1504–1513.

54 R. Manne, M. Miller, A. Duthie, M. F. da Silva, E. Y. Tshuva and T. S. Baul, Cytotoxic homoleptic Ti (IV) compounds of ONO-type ligands: synthesis, structures and activity, *Dalton Trans.*, 2019, **48**, 304–314.

55 M. N. Uddin, S. Khandaker, M. S. Amin, W. Shumi, M. A. Rahman and S. M. Rahman, Synthesis, characterization, molecular modeling, antioxidant and microbial properties of some Titanium (IV) complexes of schiff bases, *J. Mol. Struct.*, 2018, **1166**, 79–90.

56 R. Kaushal, A. Thakur, A. Bhatia, S. Arora and K. Nehra, Synthesis, characterization, DNA-binding and biological studies of novel titanium (IV) complexes, *J. Chem. Sci.*, 2020, **132**, 1–7.

57 S. C. Gagieva, V. A. Tuskaev, K. F. Magomedov, M. A. Moskalenko, A. A. Pavlov, M. Y. Meshchankina, M. A. Shcherbina and B. M. Bulychev, Immobilized on MgCl 2 bis (phenoxy-imine) complexes of Ti and Zr as catalysts for preparing UHMWPE and ethylene/higher α-olefin copolymers, *Polym. Bull.*, 2022, 1–9.

58 J. Tan, N. Zhang, L. Wang, L. Chen, C. Li, Y. Jiang and J. Wang, Norbornene polymerization and copolymerization with ethylene by titanium complexes bearing pyridinium imide ligand, *Transition Met. Chem.*, 2023, **48**, 11–20.

59 M. Białek, J. Fryga, G. Spaleniak, M. A. Matsko and N. Hajdasz, Ethylene homo-and copolymerization catalyzed by vanadium, zirconium, and titanium complexes having potentially tridentate Schiff base ligands, *J. Catal.*, 2021, **400**, 184–194.

60 R. Bhaskar and S. Sarveswari, Colorimetric sensor for real-time detection of cyanide ion in water and food samples, *Inorg. Chem. Commun.*, 2019, **102**, 83–89.

61 N. Roy, U. Sen, Y. Madaan, V. Muthukumar, S. Varddhan, S. K. Sahoo, D. Panda, B. Bose and P. Paira, Mitochondria-targeting click-derived pyridinyltriazolylmethylquinoxaline-based Y-shaped binuclear luminescent ruthenium (II) and iridium (III) complexes as cancer theranostic agents, *Inorg. Chem.*, 2020, **59**, 17689–17711.

62 M. Govindarajan, S. Periandy and K. Carthigayen, FT-IR and FT-Raman spectra, thermo dynamical behavior, HOMO and LUMO, UV, NLO properties, computed frequency estimation

analysis and electronic structure calculations on α-bromotoluene, *Spectrochim. Acta, Part A*, 2012, **97**, 411–422.
63 R. Parthasarathi, J. Padmanabhan, U. Sarkar, B. Maiti, V. Subramanian and P. K. Chattaraj, Toxicity analysis of benzidine through chemical reactivity and selectivity profiles: a DFT approach, *Internet Electron. J. Mol. Des.*, 2003, **2**, 798–813.
64 H. R. Drew, R. M. Wing, T. Takano, C. Broka, S. Tanaka, K. Itakura and R. E. Dickerson, Structure of a B-DNA dodecamer: conformation and dynamics, *Proc. Natl. Acad. Sci. U. S. A.*, 1981, **78**, 2179–2183.
65 K. Tummalapalli, C. S. Vasavi, P. Munusami, M. Pathak and M. M. Balamurali, Evaluation of DNA/Protein interactions and cytotoxic studies of copper (II) complexes incorporated with N, N donor ligands and terpyridine ligand, *Int. J. Biol. Macromol.*, 2017, **95**, V1254–V1266.
66 B. Kar, U. Das, S. De, S. Pete, A. Sharma, N. Roy, A. K. SK, D. Panda and P. Paira, GSH-resistant and highly cytoselective ruthenium (II)-p-cymene-(imidazo [4, 5-f][1, 10] phenanthrolin-2-yl) phenol complexes as potential anti-cancer agents, *Dalton Trans.*, 2021, **50**, 10369–10373.
67 H. Yang, P. Tang, B. Tang, Y. Huang, X. Xiong and H. Li, Novel poly (ADP-ribose) polymerase inhibitor veliparib: biophysical studies on its binding to calf thymus DNA, *RSC Adv.*, 2017, **7**, 10242–10251.
68 N. Dasgupta, S. Ranjan, D. Patra, P. Srivastava, A. Kumar and C. Ramalingam, Bovine serum albumin interacts with silver nanoparticles with a "side-on" or "end on" conformation, *Chem.-Biol. Interact.*, 2016, **253**, 100–111.
69 D. Sood, N. Kumar, G. Rathee, A. Singh, V. Tomar and R. Chandra, Mechanistic interaction study of bromo-noscapine with bovine serum albumin employing spectroscopic and chemoinformatics approaches, *Sci. Rep.*, 2018, **8**, 16964.
70 A. Bujacz, Structures of bovine, equine and leporine serum albumin, *Acta Crystallogr., Sect. D: Biol. Crystallogr.*, 2012, **68**, 1278–1289.
71 S. Yuan, H. S. Chan and Z. Hu, Using PyMOL as a platform for computational drug design, *Wiley Interdiscip. Rev.: Comput. Mol. Sci.*, 2017, **7**, e1298.
72 M. Manimohan, R. Paulpandiyan, S. Pugalmani and M. A. Sithique, Biologically active Co (II), Cu (II), Zn (II) centered water soluble novel isoniazid grafted O-carboxymethyl chitosan Schiff base ligand metal complexes: Synthesis, spectral characterisation and DNA nuclease activity, *Int. J. Biol. Macromol.*, 2020, **163**, 801–816.
73 M. Miller and E. Y. Tshuva, Synthesis of pure enantiomers of titanium (IV) complexes with chiral diaminobis (phenolato) ligands and their biological reactivity, *Sci. Rep.*, 2018, **8**, 9705.
74 S. Sankar and G. K. Muthukaliannan, Combinatorial effect of diclofenac with piperine and D-limonene on inducing apoptosis and cell cycle arrest of breast cancer cells, *Asian Pac. J. Trop. Biomed.*, 2023, **13**, 80–92.
75 M. Subramaniyan and M. Pathak, Crystal structure, Hirshfeld surface analysis and DFT investigation of new aluminium (III) derivative: A prominent precursor of nano alumina for dye degradation and sensor material, *Polyhedron*, 2023, **246**, 116696.
76 H. Kruse, L. Goerigk and S. Grimme, Why the standard B3LYP/6-31G* model chemistry should not be used in DFT calculations of molecular thermochemistry: understanding and correcting the problem, *J. Org. Chem.*, 2012, **77**, 10824–10834.
77 C. Adamo and D. Jacquemin, The calculations of excited-state properties with Time-Dependent Density Functional Theory, *Chem. Soc. Rev.*, 2013, **42**, 845–856.
78 H. Sharma and M. Pathak, Spectroscopic, cytotoxic, radical scavenging, DNA/BSA interactions of biologically active Schiff base supported titanium (IV) derivative and its nano titania with their computational investigation, *J. Mol. Struct.*, 2024, 137708.
79 S. V. Salimath and M. Pathak, 1-Benzyl-1H-indazol-3-ol Copper (II) Derivatives as Anticancer Agents: In-vitro Interaction with DNA/BSA, DFT, Molecular Docking and Cytotoxicity on MCF7 Cells, *ChemistrySelect*, 2024, **9**, e202304565.